LLC Resonant Converter Based Single-stage Inverter with Multi-resonant Branches

Dong Jiao

Thesis submitted to the faculty of the Virginia Polytechnic Institute and State University in partial fulfillment of the requirements for the degree of

Master of Science
In
Electrical Engineering

Jih-Sheng Lai, Chair
Dong Dong
Xiaoting Jia

March 3rd, 2022
Blacksburg, VA

Keywords: single-stage inverter, LLC resonant converter, multi-resonant, higher order harmonics, variable-frequency-modulation, ZVS

LLC Resonant Converter Based Single-stage Inverter with Multi-resonant Branches

Dong Jiao

ABSTRACT

This paper presents a single-stage inverter with variable frequency modulation (VFM) based on LLC resonant converter. And LLC converter is a common topology of dc/dc conversion. LLC resonant converter can achieve high efficiency and soft-switching performance. Since the dc gain curve of the single-resonant LLC converter is flat when the switching frequency is larger than the resonant frequency, namely $f_s > f_r$, an additional L-C series resonant branch is paralleled to the original resonant tank to introduce higher-order-harmonic resonant current and a zero-gain point to the gain curve. Higher-order-harmonics help to deliver power and the zero-gain point enlarges the gain range which improves output THD and reduces the switching frequency range.

A 1.2 kW prototype is built to demonstrate the performance of the proposed inverter. Zero-voltage-switching (ZVS) and zero-current-switching (ZCS) are achieved on the primary side and secondary side, respectively. And 97.3% efficiency and 2.17% voltage THD are achieved at full load condition, while 97.2% efficiency and 3.2% voltage THD are achieved at half load condition.

Single-stage LLC Inverter by Using Multi-resonant Branches

Dong Jiao

GENERAL AUDIENCE ABSTRACT

The inverter is widely used to connect renewable energy into the grid by converting dc to ac waveform, like photovoltaic (PV) technology. Basically, the two-stage topology is usually used. The inverter would consist of two stages working in high frequency, the first stage is dc/dc converter which can regulate the input voltage to the desired bus voltage for the second stage, and the second stage is dc/ac converter. The first stage works at a specific switching frequency, so it can be designed to achieve higher efficiency in dc/dc conversion. The second stage also works at high switching frequency and converts dc to ac commonly by using SPWM which changes the duty cycle ratio in a sinusoidal pattern. The single-stage inverter only has one stage working in high frequency while the second stage works at twice line frequency. The first stage converts dc to rectified ac waveform and the second stage unfolds it to ac.

The topology of LLC resonant converter being applied for the first stage of the single-stage inverter has been proposed. This topology uses variable-frequency-modulation (VFM) which varying switching frequency on the primary side to output different voltage levels. And it achieves zero-voltage-switching (ZVS). However, LLC converter can hardly output very low voltage due to the flat voltage gain curve at high frequency. Also, LLC converter only transfers the fundamental harmonic component to the load. If the higher-order harmonic components help transfer power when the

switching frequency equals the resonant frequency, the current shape will be more like a square wave and the peak of resonant current can be reduced.

This thesis proposes a topology that has two L-C resonant branches in parallel for the resonant tank in the converter. And the paralleled resonant branches produce a zero-gain frequency point into the gain curve so that the gain range is enlarged within the reduced switching frequency range and 3rd harmonic component of the resonant current helps to transfer power so that the rms value of resonant current can also be reduced.

To my parents,

Zheng-Qi Jiao

Gui-Yin Zhong

Acknowledgements

First and foremost, I would like to sincerely thank my advisor, Dr. Jih-Sheng Lai, it is a great privilege to study at Future Energy Electronics Center (FEEC) and under his guidance and supervision. I benefited a lot from his personality and diligence. And I am grateful for Dr. Dong Dong, Dr. Xiaoting Jia, and Dr. Wei Zhou to serve as my committee members.

I also express my appreciation to all teachers who have lectured me for their insightful lectures which are of great benefit to me in my research.

The experimental test is never a solo work, so I want to acknowledge Dr. Hao Wen for supporting and working with me through the propagation research. Also, I would like to appreciate Dr. Chih-Shen Yeh, Dr. Moonhyun Lee, Dr. Cheng-Wei Chen, Dr. Oscar Yu, Dr. Yong Liu, Dr. AnhDung Nguyen, Mr. HsinChe Hsieh, Mr. Eric Chu, Mr. Zheng-Ming Hou, Mr. Bryan Gutierrez, Ms. Fran Gailie from FEEC.

Finally, I would like to express my deep appreciation to my family and my girlfriend for their love, encouragement, and understanding throughout my pursuit of the master's degree.

I hope the Covid pandemic will end soon.

Table of Contents

Chapter 1 Introduction 1

1.1 Background 1

1.1.1 Multi-stage Inverters and Single-stage Inverters 1

1.1.2 Single-stage Inverters Based on LLC Resonant Converter 3

1.2 Research Object 9

Chapter 2 Topology and Operation 11

2.1 Proposed Topology 11

2.1.1 FHA Model and Transfer Function 12

2.1.2 Wide Gain Range 13

2.1.3 Power Delivery by Utilizing 3rd harmonics 16

2.2 Control Strategy 17

Chapter 3 Prototype Design and Implementation 18

3.1 Resonant Tank Design 18

3.1.1 Operation Frequency Selection 18

3.1.2 Weight Ratio between Currents from Two LC Branches 20

3.1.3 Leakage Inductor Effect 22

3.2 ZVS Performance 24

3.3 Design methodology 27

3.4 Simulation Verification 28

Chapter 4 Experiments Results and Loss Analysis 34

4.1 Test Result dc/dc 34

4.2 Test Result dc/ac 36

4.3 Loss Breakdown 37

Chapter 5 Conclusions and Future Work 40

5.1 Conclusions 40

5.2 Future Work 41

Reference 43

List of Figures

Figure 1.1 Two-stage inverter 2

Figure 1.2 Single-stage inverter 2

Figure 1.3 LLC circuit 5

Figure 1.4 Equivalent circuit of LLC converter 5

Figure 1.5 Gain curves and operation regions of LLC converters 6

Figure 1.6 Gain curves of LLC converter at different load conditions 6

Figure 1.7 Control strategy of LLC based single-stage inverter 7

Figure 1.8 FB+HB VFM control strategy 7

Figure 1.9 Gain curves and expected output waveforms of full-bridge mode and half-bridge mode modulation respectively 8

Figure 1.10 Waveforms and power delivery analysis 8

Figure 2.1 Multi-resonant LLC circuit 11

Figure 2.2 FHA model of proposed topology 12

Figure 2.3 Voltage gain curve of multi-resonant LLC circuit 14

Figure 2.4 Gain curves of single-resonant LLC and multi-resonant LLC 15

Figure 2.5 Voltage gain curves with different resonant inductors 15

Figure 2.6 current waveforms with same unity amplitude 16

Figure 2.7 Simpler control method for proposed topology 17

Figure 3.1 Gain curves with different f_3 selection 19

Figure 3.2 Gain curve of case 2 based on PSIM simulation 20

Figure 3.3 Simplified circuit for L-C branch 20

Figure 3.4 Resonant current comparison between single-resonant LLC and multi-resonant LLC at f_s=f_r in dc/dc conversion 22
Figure 3.5 Weight ratio between currents from two LC branch of multi-resonant LLC.. 22
Figure 3.6 New FHA model of proposed topology 23
Figure 3.7 ZVS issue at low output voltage..... 25
Figure 3.8 Voltage gain curves with different zero-point frequency..... 25
Figure 3.9 ZVS conditions at same output voltage with different zero-gain frequency... 26
Figure 3.10 Voltage gain curves with different load condition 28
Figure 3.11 Updated multi-resonant LLC..... 30
Figure 3.12 Comparison between single-resonant LLC and multi-resonant LLC with dc/dc simulation at resonant frequency (a) at full load condition; (b) at half load condition 31
Figure 3.13 Two current components in two resonant branches from dc/dc simulation at full load condition at resonant frequency in multi-resonant LLC..... 32
Figure 3.14 dc/ac simulation results (a) at full load condition; (b) at half load condition 33
Figure 4.1 dc/dc test at f_s=344 kHz at full load condition 35
Figure 4.2 dc/dc test at f_s=635 kHz at full load condition 35
Figure 4.3 dc/ac test result at full load condition (1.2 kW) 36
Figure 4.4 dc/ac test result at half load condition (600 W)..... 37
Figure 4.5 Mn-Zn ferrite core loss data from Hitachi Metals..... 38

List of Tables

Table 3.1 Resonant elements parameters 30

Table 3.2 Resonant current rms value comparison between single-resonant LLC and multi-resonant LLC at $f_s=f_r$ 30

Table 4.1 Additional components selection 34

Table 4.2 Summary of power stage components losses 38

Table 4.3 Loss breakdown 39

Chapter 1 Introduction

1.1 Background

Power electronics is developing rapidly, and the inverter is widely used in many applications of daily life, including the computer, communication, power system, aerospace, and so on. Inverters convert dc to ac waveform through switching operation of semiconductor power switch devices. Among the existing power sources, common dc sources include battery and photovoltaic (PV), and inverters should be applied if the load needs ac input.

1.1.1 Multi-stage Inverters and Single-stage Inverters

Inverters can be basically classified into two sorts, which are multi-stage inverters and single-stage inverters. Some merits and demerits of different inverter strategies have been discussed in [1][2]. Multi-stage inverters commonly use dc/dc + dc/ac topology, as presented in

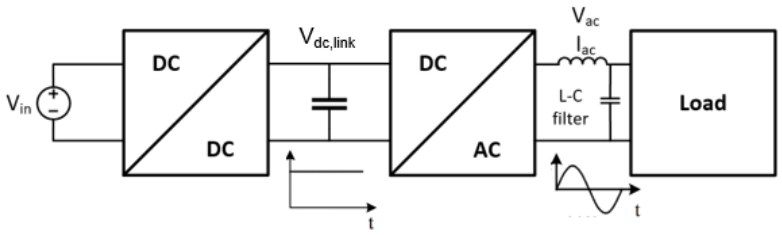

Figure 1.1, a dc/dc converter together with a voltage source inverter (VSI) or current source inverter (CSI) is commonly used in connecting PV to the utility grid. This topology can achieve high efficiency since dc/dc converter can be optimized to work at maximum-efficiency frequency and VSI or CSI with proper input and controller can also achieve maximum efficiency and good performance.

To convert dc voltage to a sinusoidal waveform, the sinusoidal pulse width modulation (SPWM) technique is commonly used [3]. With a fixed switching frequency, the sinusoidal waveform is created by varying the duty duration of each cycle that the positive voltage is applied. By using SPWM, we can expect similar THD of output ac voltage under different load conditions. Also, a L-C filter is required to smooth the output sinusoidal waveform. Thus, the single-stage inverter can save the bulky dc-link capacitor and L-C filter.

And single-stage inverters usually use dc/rectified ac + unfolding topology, as presented in

Figure 1.2. Basically, single-stage topology can use the same circuit with two-stage topology [4]. However, in single-stage topology, only the first stage switches at high switching frequency to convert dc to rectified ac, and the second stage is to unfold rectified ac into ac wave.

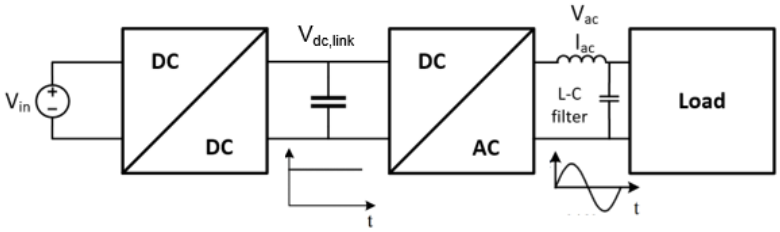

Figure 1.1 Two-stage inverter

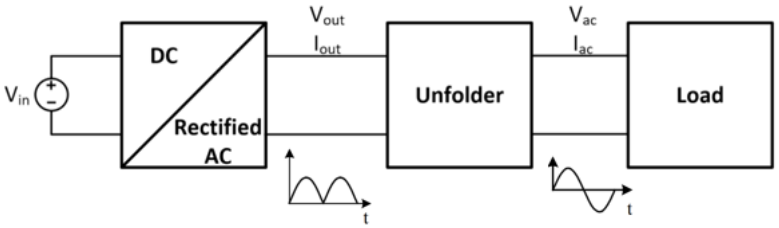

Figure 1.2 Single-stage inverter

The unfolding stage switches at twice line frequency and only switches at voltage zero-crossing so that the switching loss from the unfolding stage can be ignored. And in a two-stage topology, a large bus capacitor should be placed after dc/dc converter as energy storage to attenuate 120 Hz ripple from the output side [5]. Single-stage topology uses a small filter capacitor instead of a bulky bus capacitor since the output of the first stage is not constant but variant.

Conventional single-stage inverters, including buck inverter, boost inverter, buck-boost inverter which are using pulse density modulation (PDM), frequently suffer from the low range of input voltage, component counts, control complexity, efficiency, and power density. Reference [6] uses a flyback converter to achieve dc – rectified sinusoidal wave. And reference [7] adopts a Cuk converter. Many other single-stage inverter topologies [8][9][10][11][12] are presented with demerits and merits. For the converters using PWM modulation method, hard-switching operation results in a low efficiency. And rms value of resonant current is high when the duty cycle is low at low line output because the conduction time in one single cycle is short [13].

To improve the waveform quality, multi-module stacking can be applied to both two-stage topology and single-stage topology. References [14][15] proposed the concepts of the multi-level inverter, and better THD of the output voltage can be achieved with the increased number of stacked modules.

1.1.2 Single-stage Inverters Based on LLC Resonant Converter

LLC resonant converter is widely used in dc/dc conversion due to simple topology, high efficiency [16][17][18][19]. The LLC circuit topology, equivalent circuit and control strategy are presented in Figure 1.3, Figure 1.4, Figure 1.5 and Figure 1.8.

LLC resonant converter can achieve zero-voltage-switching (ZVS) at primary side devices and zero-current-switching (ZCS) at secondary side devices, which saves switching loss. Basically, the LLC resonant converter is used in dc/dc conversion since it can be easily optimized at one single operating point. At the region that $f_s > f_r$, with low voltage output, the primary side of converter may lose ZVS. The other shortcoming of inverters based on LLC resonant converter is the flat voltage gain curve at high frequency so that the low output voltage is hard to be achieved. And Figure 1.6 presents the gain curves of LLC converter at half load condition in the orange curve and full load condition in the blue curve. Under lighter load conditions, the gain at high switching frequency is even higher which results in an even narrower gain range and worse THD of the output ac voltage. The high switching frequency would result in high core loss in magnetic components, like inductors and the transformer. In Figure 1.6, with the range of 340kHz to 1.2MHz that the maximum switching frequency is nearly 4 times of the minimum switching frequency, the gain range is from 0.22 – 1 in the full load condition while the gain range is from 0.36 – 1 in the half load condition.

To achieve wider gain range that outputs lower voltage at the high switching frequency, the half-bridge modulation method can be applied. Figure 1.7 and Figure 1.8 shows the hybrid control strategy. Output voltage is sensed and compared with a preset sinusoidal wave reference. And a simple PI controller is applied to adjust the switching frequency and the gain. In the region 1, full-bridge mode can be applied for high line region and in the region 2, half-bridge mode can be applied for low line region [20]. And in the region 3, the power stage is shut down and the THD is sacrificed while the efficiency can be saved. By applying half-bridge modulation method, the voltage gain

can be halved which is presented in Figure 1.9. The output gain is 0.36 at 1.2 MHz in the full-bridge mode then the gain equals to 0.18 at 1.2 MHz in the half-bridge mode. With the gain range of the half load condition compared to the full load condition, the THD of the expected output waveform can be improved from 10.1% to 3.92%. Thus, the hybrid modulation method could be a good solution for the wide-range ZVS and wide-range gain.

Inverters based on LLC resonant converter use variable frequency modulation (VFM) [21]. The rms value of resonant current is lower at low line region. However, LLC resonant converter could generate more circulating energy.

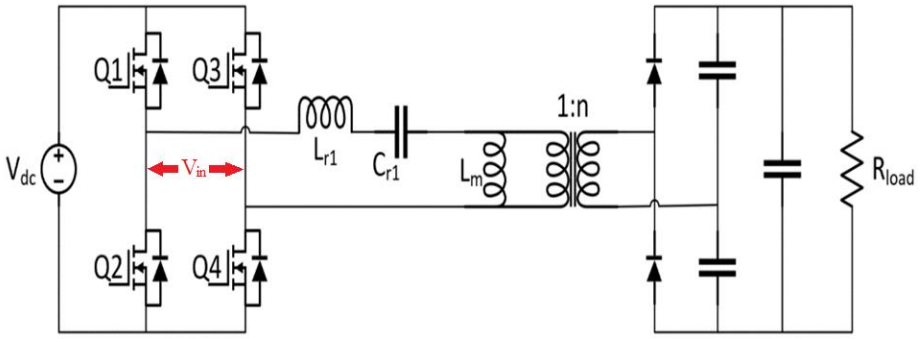

Figure 1.3 LLC circuit

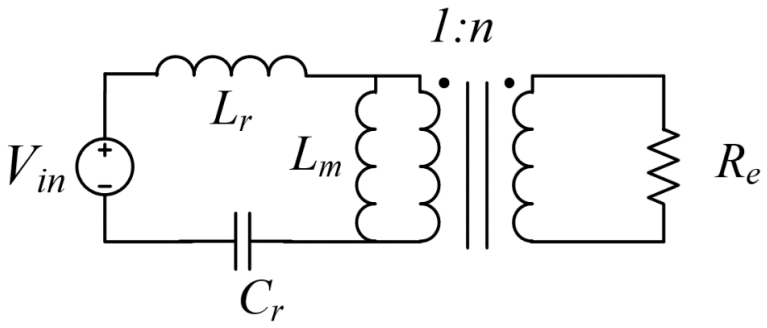

Figure 1.4 Equivalent circuit of LLC converter

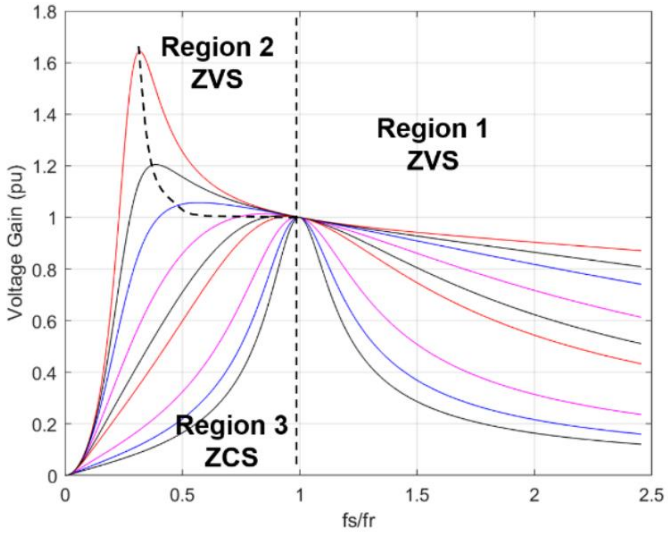

Figure 1.5 Gain curves and operation regions of LLC converters

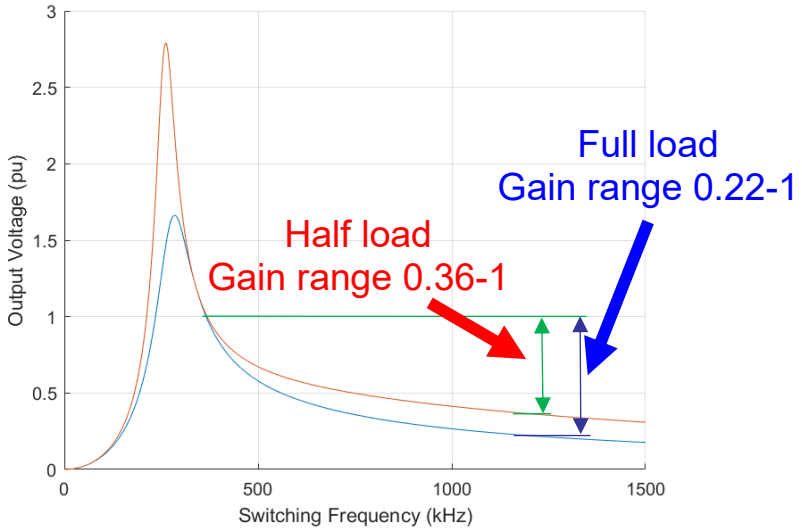

Figure 1.6 Gain curves of LLC converter at different load conditions

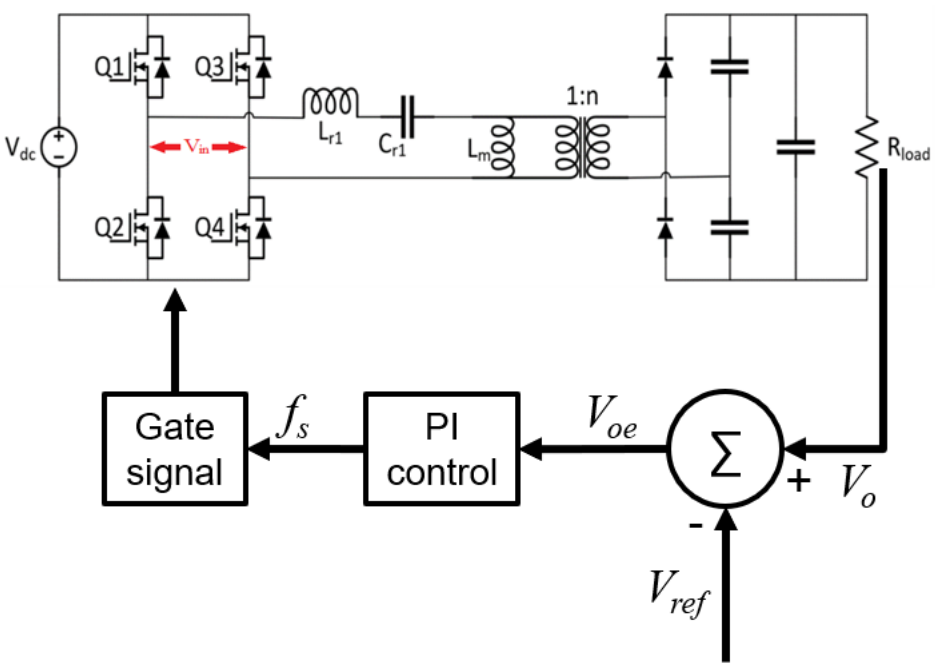

Figure 1.7 Control strategy of LLC based single-stage inverter

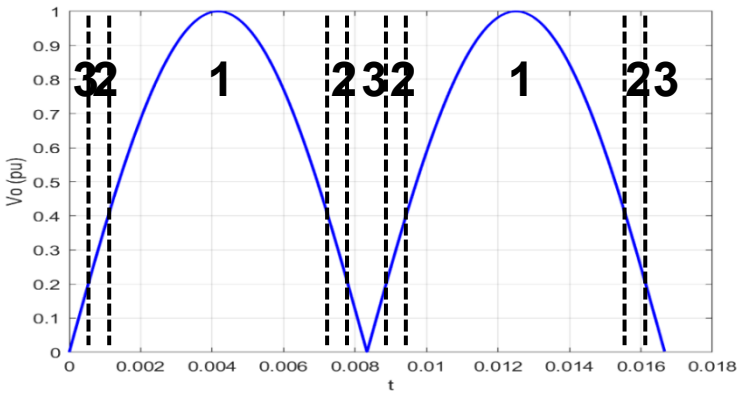

Figure 1.8 FB+HB VFM control strategy

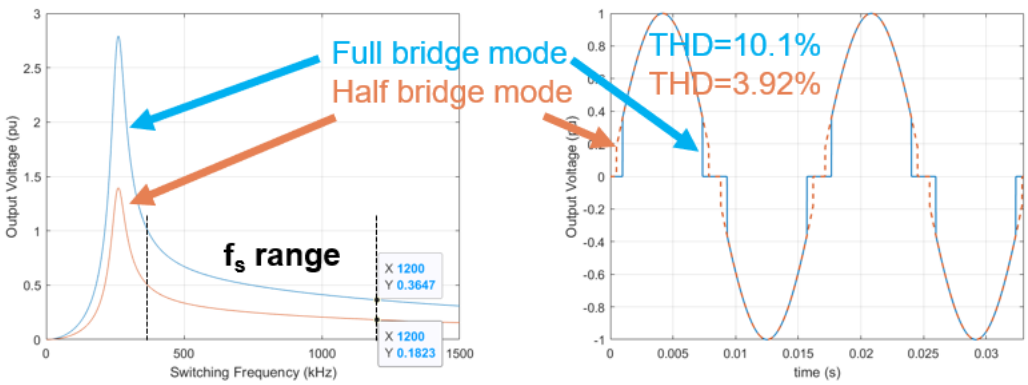

Figure 1.9 Gain curves and expected output waveforms of full-bridge mode and half-bridge mode modulation respectively

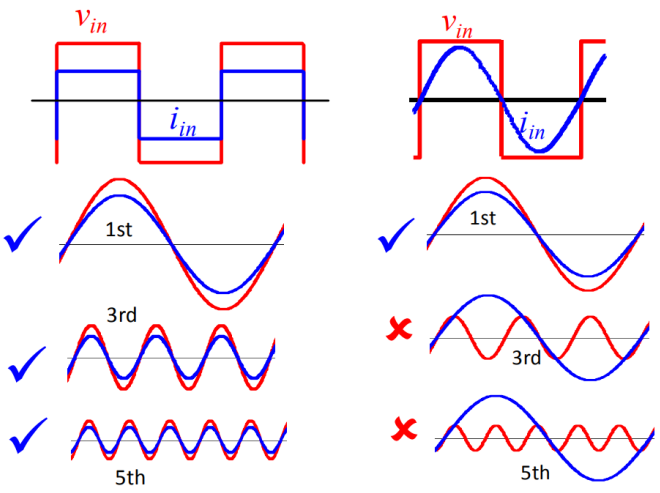

(a) (b)

Figure 1.10 Waveforms and power delivery analysis

The resonant tank can be considered as a low-pass filter which can filter the higher-order harmonics components. Essentially, only the fundamental component can be allowed to flow through the resonant tank which delivers the power to the load. And the resonant current is also a sinusoidal wave so that the higher-order harmonics components of the square-wave V_{in} does not contribute to the power transferring. In the left side of Figure 1.10, the current and voltage are both square waveforms, and the square waveforms can be decomposed as a combination of odd harmonics according to the

Fourier Analysis, so virtually no circulating energy is generated [22]. For the resonant converter, the primary side voltage is a square waveform, and the current is a sinusoidal waveform that is presented on the right side of Figure 1.10, the higher order of harmonics of voltage and current exhibit reactive power [23].

Inverters based on LLC resonant converter have demerits as followed:

(1) The voltage gain curve is flat at high frequency, and with lighter load conditions, the gain at high frequency is even higher so that the gain range is narrower or higher switching frequency is needed to achieve low output.

(2) Full bridge + half bridge VFM control method is not very easy.

(3) Only the fundamental component is delivered to the load and the higher-order harmonics generate the circulating energy.

The multi-resonant branches strategy based on LLC converter [24] has been proposed in dc/dc conversion. For easily distinguish, LLC converter using multi-resonant branches would be called as the multi-resonant LLC converter, and conventional LLC resonant converter would be stated as the single-resonant LLC converter. With the proposed topology, at $f_s > f_r$ in dc/dc conversion, the resonant current is reshaped as a semi-rectangular waveform by combining a limited number of higher-order odd harmonics of fundamental resonant frequency, and current rms is increased and the current peak is induced, and power density is improved.

1.2 Research Object

This research aims to build a single-stage inverter based on LLC resonant converter. However, an inverter using the conventional single-resonant LLC converter has some demerits which are mentioned in the previous section. For the first and second

demerits, a zero-gain frequency point can be created and added into the voltage gain curve so that the switching frequency range can be narrower, and the control method can be easier. And for the third demerit, higher order harmonic component can be introduced to help deliver power. Then the peak of the resonant current can be decreased at $f_s=f_r$ in dc/dc conversion. Thus, a single-stage inverter using multi-resonant branches is proposed.

Chapter 2 Topology and Operation

2.1 Proposed Topology

The proposed multi-resonant LLC circuit is presented in Figure 2.1. The difference between the single-resonant LLC converter and the proposed multi-resonant LLC converter is the resonant tank. An additional L-C branch is paralleled with the resonant tank of the single-resonant LLC converter. Devices *Q5 – Q8* are the unfolding stage works at 120 Hz which is twice line frequency. L_{r1} and C_{r1} resonant at the fundamental frequency, and L_{r3} and C_{r3} resonant at the third harmonic frequency.

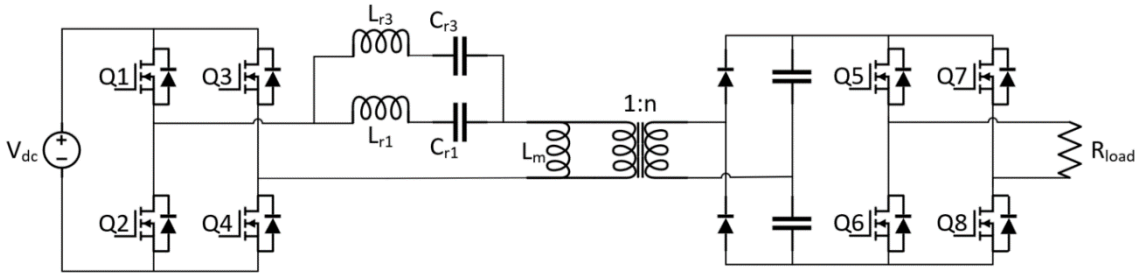

Figure 2.1 Multi-resonant LLC circuit

The topology of resonant converter with multiple passive components has been stated in some papers. The principle of the multi-element resonant converter is to create several different resonant frequencies and to utilize the higher-order harmonics components to reduce the circulating energy [22][25][26][27][28] in dc/dc conversion. Like the conventional single-resonant LLC converter, the multi-element resonant converter can be optimized at a single operating point. Reference [24] introduces the topology with multi-resonant branches and optimizes the resonant current to be semi-rectangular wave to maximum power density and minimize peak current.

2.1.1 FHA Model and Transfer Function

To the proposed converter, the fundamental harmonic approximation (FHA) analysis is applied, the equivalent circuit is shown in Figure 2.2. Each L-C branch is responsible for a specific resonant frequency. FHA methodology is widely used in the resonant converter analysis [29]. FHA assumes that only the fundamental component of the voltage input which is a square wave is delivered to the output. The advantage of FHA is that it is simple to apply and easy to understand. Meanwhile, the issue of FHA method is that it is only accurate when f_s=f_r since the method is based on the fundamental harmonic and large error will occur when the switching frequency is far away from the resonant frequency [30][31]. Reference [32] presents a set of more accurate equations based on time interval analysis (TIA) which can also be used to predict the performance of LLC circuit, like the resonant current. And reference [33] introduces a model with equivalent L_m to predict the performance of an LLC converter based on time domain analysis. Even so, the FHA method can be used for the tendency of the performance of the proposed converter.

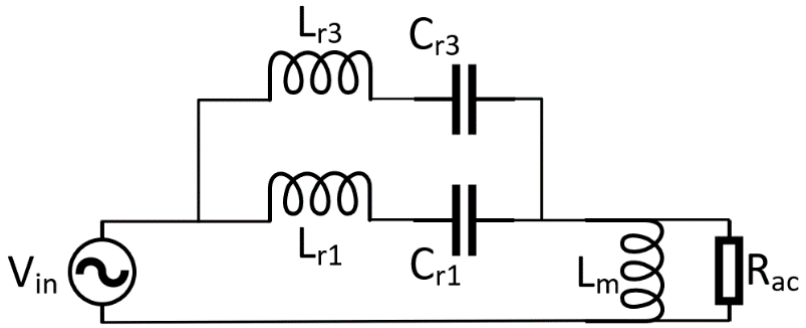

Figure 2.2 FHA model of proposed topology

2.1.2 Wide Gain Range

The voltage gain curves under different load conditions are presented in Figure 2.3 based on FHA methodology. With different load conditions, the gain curves are shown. With an additional LC branch, a zero-gain frequency point is introduced into the gain curve so a wide gain range can be achieved with a limited frequency range. The switching frequency range is circled with dot-line rectangular. The linear gain curve is preferred in the region which is good for the control method so that the red curve in Figure 2.3 is set as the full load condition. The two unity-gain frequency points are from the resonant frequency of two branches, respectively. The zero-gain frequency point is based on the two L-C branches resonant tank.

$$f_1 = \frac{1}{2\pi\sqrt{L_{r1}C_{r1}}} \qquad (2-1)$$

$$f_2 = \frac{1}{2\pi\sqrt{(L_{r1}+L_{r3})\left(\frac{C_{r1}C_{r3}}{C_{r1}+C_{r3}}\right)}} \qquad (2-2)$$

$$f_3 = \frac{1}{2\pi\sqrt{L_{r3}C_{r3}}} \qquad (2-3)$$

Thus, the switching frequency range is between f_1 and f_2 which is much narrower that the switching frequency range of LLC-based inverter. As presented in Figure 2.4, the orange curve shows the gain curve of conventional single-resonant LLC converter while the blue curve is the gain curve of the proposed multi-resonant converter. From the gain curve, proposed multi-resonant LLC converter achieves wider gain range with a limited frequency range compared to conventional single-resonant LLC converter. Narrower switching frequency range is better for magnetic material selection and also can save magnetic loss.

The gain curve of the proposed multi-resonant LLC converter has a zero-gain point so the converter can reach zero voltage output theoretically. However, zero gain cannot be reached because the gain curve shown in Figure 2.4 is based on FHA analysis method which means only the fundamental component can reach zero while the higher-order harmonics will contribute to the voltage gain. And with lighter load condition, the 3rd harmonics gain is higher, so the real gain range of lighter load condition is narrower.

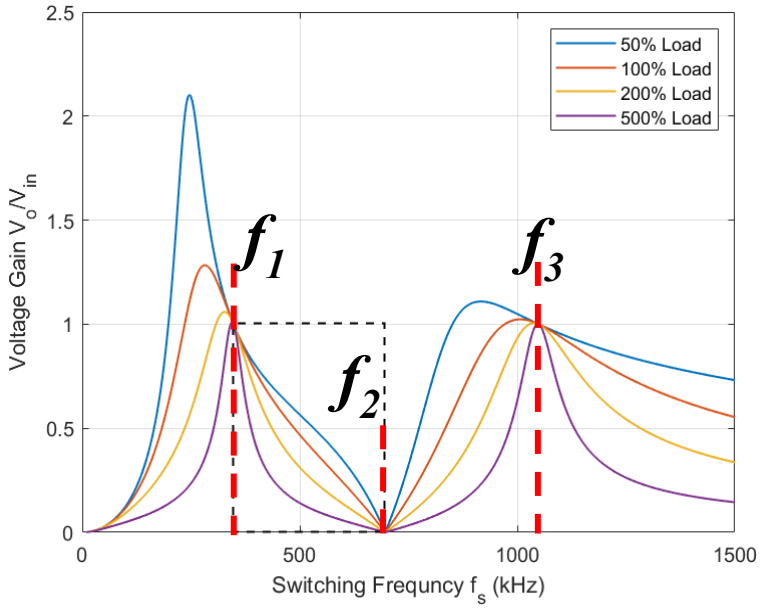

Figure 2.3 Voltage gain curve of multi-resonant LLC circuit

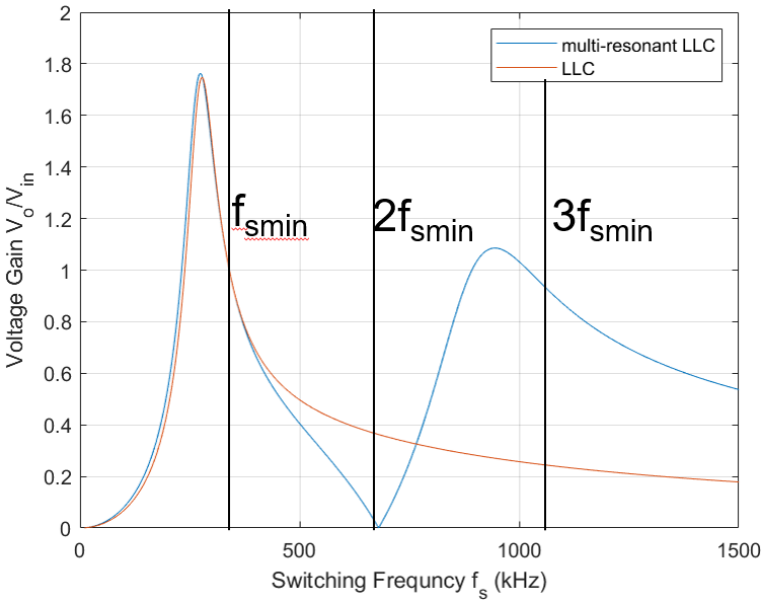

Figure 2.4 Gain curves of single-resonant LLC and multi-resonant LLC

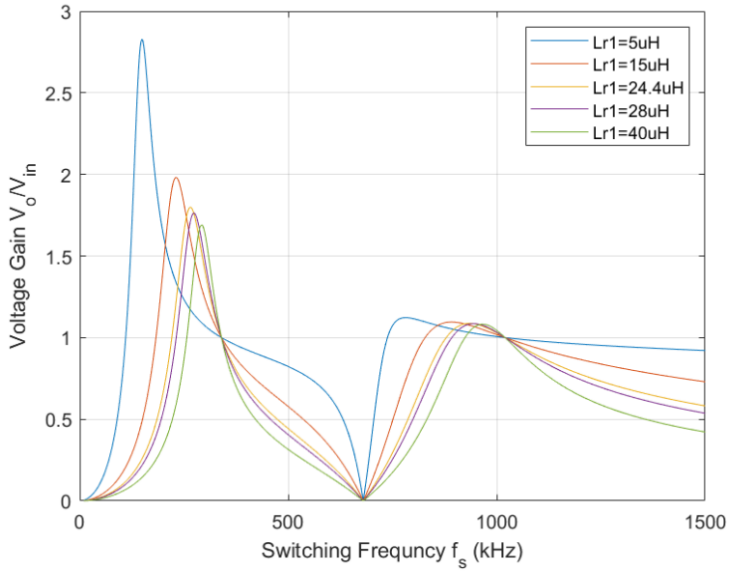

Figure 2.5 Voltage gain curves with different resonant inductors

To reduce the effect of the 3rd harmonics at high switching frequency, there are two solutions which are decreasing the amplitude of the 3rd harmonics component and decreasing the phase difference of two harmonics components. A model can be

developed in the future to predict and control the phase difference between two harmonics components.

2.1.3 Power Delivery by Utilizing 3rd harmonics

Moreover, the additional LC branch brings another merit which is utilizing the 3rd order harmonics current component to help deliver power. Figure 2.6 presents an example of two current waveforms with same amplitude but different average value. Current i_1 only has fundamental component while current i_2 consists of fundamental and 3rd order harmonics. With the same amplitude, i_2 has 22% larger average value than i_1. Therefore, with same power level, utilizing 3rd order harmonics can reduce the amplitude and rms of resonant current.

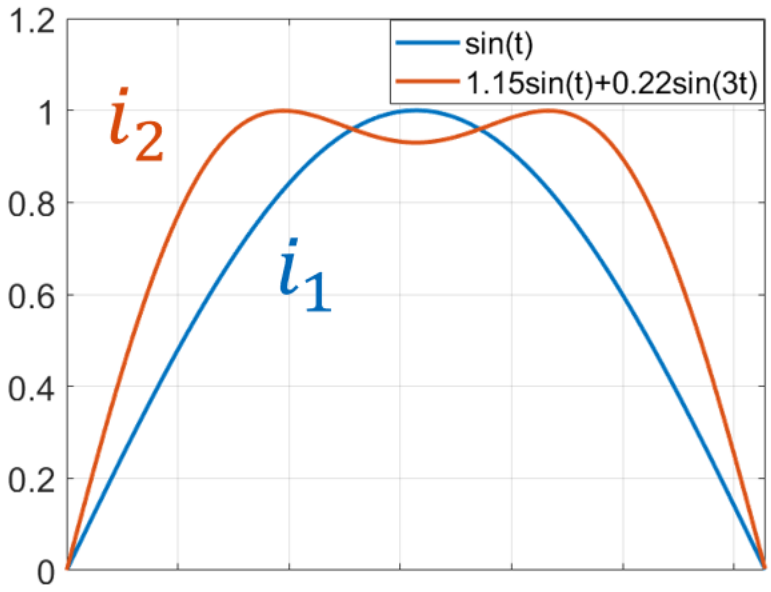

Figure 2.6 current waveforms with same unity amplitude

2.2 Control Strategy

Since the gain curve has a zero-gain point, the proposed topology can achieve a quiet low output voltage, the control method only consists of two modes instead of three modes, which is presented in Figure 2.7. In region 1, full-bridge mode VFM can be applied, and the power stage is shut down in region 2 with the same reason that sacrificing THD and save the efficiency. Since full-bridge mode VFM modulation can be applied to whole line region, the control strategy is simpler than the hybrid full-bridge + half-bridge mode.

The control methodology is simple that only a voltage sensor at the output is needed. Set a sinusoidal reference wave and apply a PI controller to adjust the switching frequency to track the reference shape.

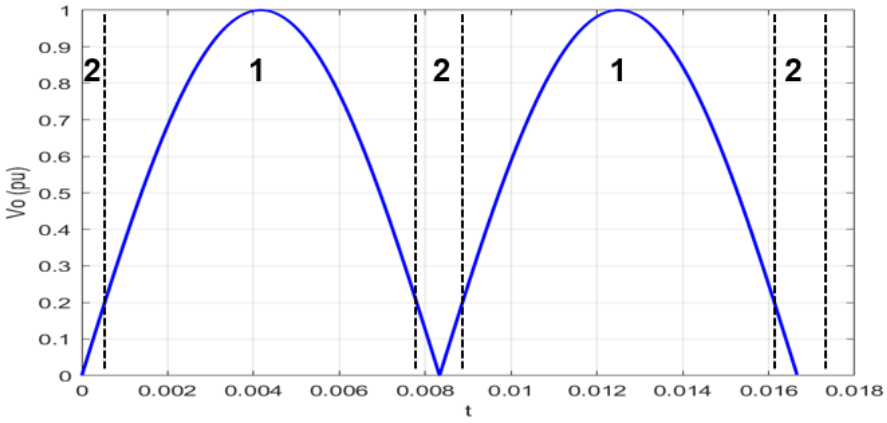

Figure 2.7 Simpler control method for proposed topology

Chapter 3 Prototype Design and Implementation

3.1 Resonant Tank Design

3.1.1 Operation Frequency Selection

The gain curves under different load conditions are shown in Figure 2.3. And the operation frequency region is selected from f_1 to f_2 because ZVS can be achieved when the slope of gain curve is negative in LLC resonant converter.

The input voltage across two middle points of the full bridge primary side is excited as a square waveform. According to the Fourier analysis, the square waveform only has odd harmonics. Odd harmonics transfer power and zero-gain frequency should be kept away from the odd harmonics of the resonant frequency. Thus, to avoid circulating energy at nominal condition, pick the zero-gain frequency at around even times of the resonant frequency, namely $f_2 \approx 2f_1$.

Then f_3 should be designed according to the effect of 3rd order harmonics. Like case 1 in Figure 3.1, the gain curves in the switching frequency range and the 3rd harmonics range are both monotonic so that the voltage gain of the proposed converter is monotonic and good for the control. Otherwise, like case 2 in Figure 3.1, the gain curve in the 3rd harmonics range is not monotonic if the second peak gain point is larger than the triple fundamental frequency which is in the 3rd harmonics range. The gain is larger in case 2 than that in case 1. Since the gain curves in switching frequency range and 3rd

harmonics range are not both monotonic so that it is hard to determine whether the combination of the fundamental frequency component and the 3rd harmonics component is monotonically decreasing with frequency growing. Based on the simulation, Figure 3.2 shows the gain curve based on case 2 in Figure 3.1 at half load condition, and the gain curve is not monotonically decreasing with the increasing switching frequency, for example, the voltage gain at f_s=500kHz is larger than the voltage gain at f_s=480kHz. And the output voltage and the resonant current waveforms are shown in Figure 3.2. Thus, the second peak gain point should be designed less than the triple fundamental frequency to maintain the gain curve of the proposed converter to be monotonic, $f_3 \leq 3f_1$.

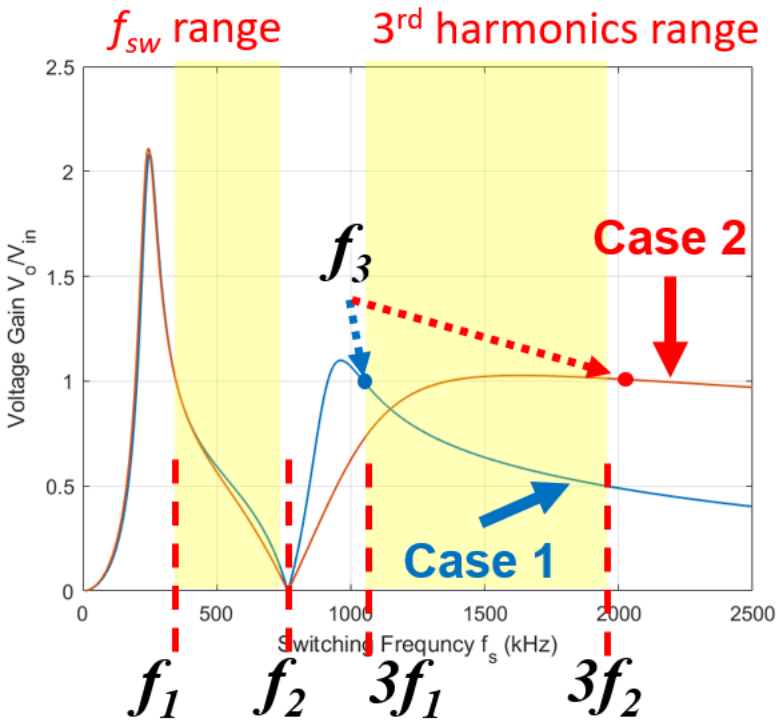

Figure 3.1 Gain curves with different f_3 selection

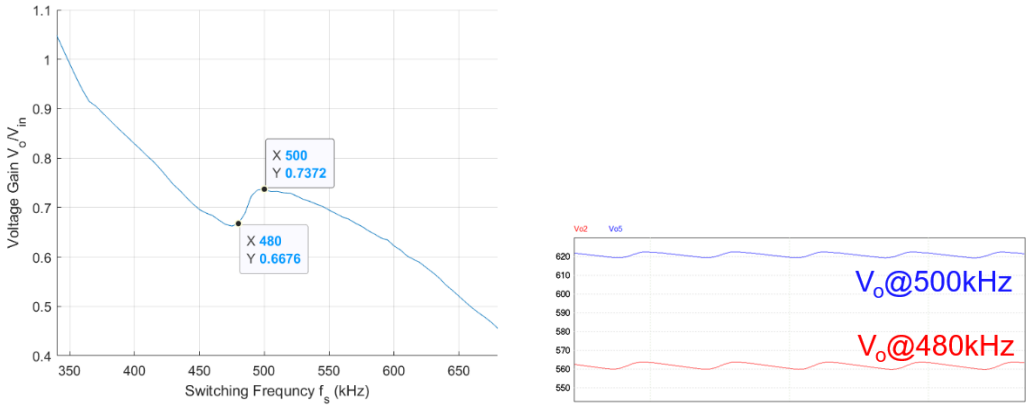

Figure 3.2 Gain curve of case 2 based on PSIM simulation

3.1.2 Weight Ratio between Currents from Two LC Branches

Based on the size of the inductor and capacitor in different branches, the weight ratio of the current through different branches can be determined [24]. Assume that the different resonant branches are independent in generating the resonant current. And same voltage is applied across different L-C branches, a simplified circuit can be applied for all of them, which is presented in Figure 3.3.

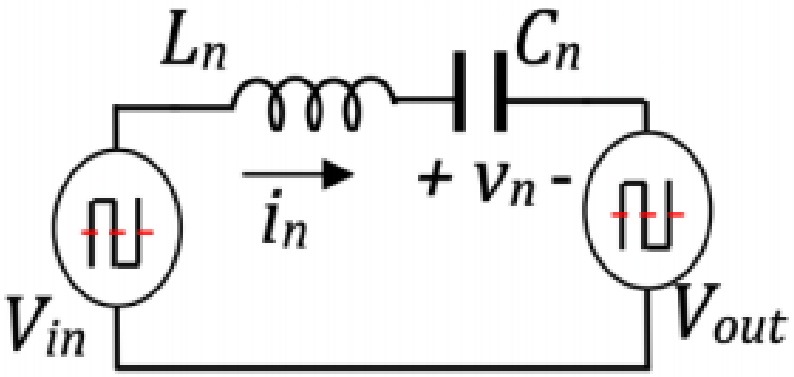

Figure 3.3 Simplified circuit for L-C branch

The time-domain equations of the voltage across the capacitor and the current going through L-C branch are shown in equation (3-1) and (3-2).

$$L_n \frac{di_n}{dt} = V_{in} - V_{out} - v_n = V_e - v_n \qquad (3-1)$$

$$C_n \frac{dv_n}{dt} = i_n \qquad (3-2)$$

Converting the two equations to the frequency domain, then equation (3-3) and (3-4) are presented.

$$sL_n I_n = \frac{|V_e|}{s} - V_n \qquad (3-3)$$

$$sC_n V_n = I_n \qquad (3-4)$$

And then the magnitude of the current can be written below and $\omega_n = \frac{1}{\sqrt{L_n C_n}}$.

$$I_n = \frac{|V_e|}{L_n \omega_n} \frac{\omega_n}{s^2 + \omega_n^2} \qquad (3-5)$$

And the $\frac{\omega_n}{s^2+\omega_n^2}$ term represents the sinusoidal signal with frequency ω_n, so that the $\frac{|V_e|}{L_n \omega_n}$ represents the magnitude of the current. Thus, the weight ratio of current from two branches is as followed in equation (3-6). The item $I_{r3,p}$ is the magnitude of current through the 3rd harmonic branch, and the item $I_{r1,p}$ is the magnitude of current through the fundamental harmonic branch.

$$\frac{I_{r3,p}}{I_{r1,p}} = \frac{\frac{|V_e|}{L_{r3}\omega_3}}{\frac{|V_e|}{L_{r1}\omega_1}} = \frac{L_{r1}\omega_1}{L_{r3}\omega_3} \qquad (3-6)$$

A simulation is done to verify this equation. Figure 3.4 presents the performance comparison between single-resonant LLC and multi-resonant LLC. The multi-resonant LLC is not optimized but adding a LC branch directly to an existing single-resonant LLC. And with the help of 3rd harmonics, multi-resonant LLC has lower rms value in resonant current. Then split the resonant current of multi-resonant LLC into fundamental and 3rd

harmonics components which is shown in Figure 3.5. From the simulation result, the weight ratio between currents from two LC branches is $\frac{I_{r3,peak}}{I_{r1,peak}} = 0.54$, and from equation (3-6), the result is $\frac{L_{r1}\omega_1}{L_{r3}\omega_3} = 0.55$ which can match the simulation result.

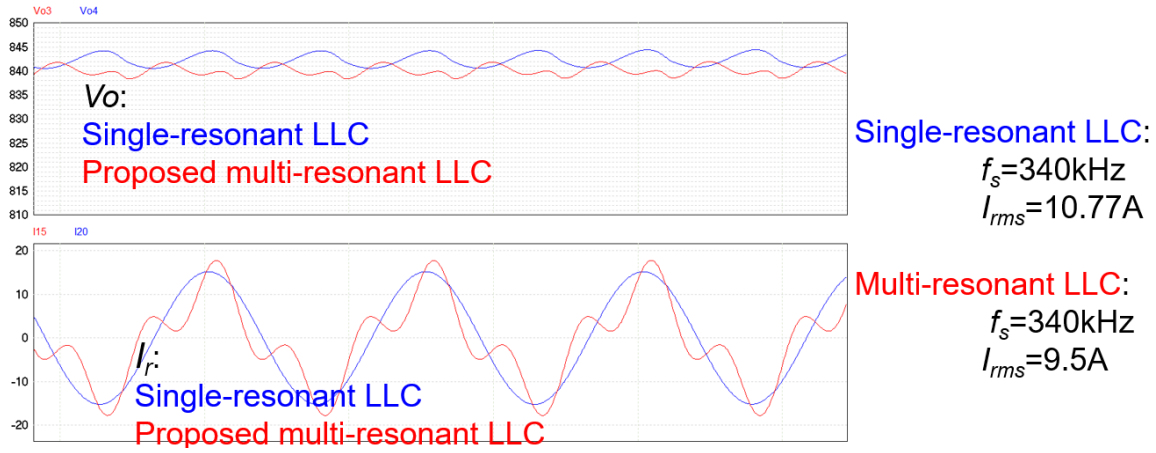

Figure 3.4 Resonant current comparison between single-resonant LLC and multi-resonant LLC at f_s=f_r in dc/dc conversion

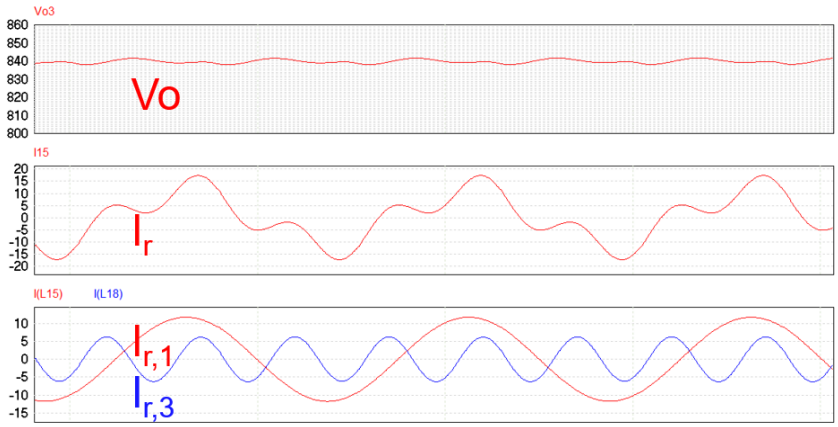

Figure 3.5 Weight ratio between currents from two LC branch of multi-resonant LLC

3.1.3 Leakage Inductor Effect

Determine the zero-gain frequency point:

$$f_2 = xf_1 \qquad (3-7)$$

Combined equations (2-1) (2-2) (2-3) (3-7), the relation between two resonant inductors is presented in equation (3-8).

$$L_{r3} = \frac{x^2 - 1}{9 - x^2} L_{r1} \qquad (3-8)$$

Then if x is picked as 2, equation (3-8) can be written as $L_{r3} = \frac{3}{5} L_{r1}$. Thus, the ratio of two resonant inductors determines the weight ratio of the current components and the zero-gain frequency point.

In addition, the leakage inductance of the transformer should also be considered in the design. Techniques to minimize the leakage inductance are presented in reference [34]. In the conventional LLC resonant converter, the leakage inductance of the transformer can be involved in the resonant inductance easily. Likewise, in the proposed topology, the leakage inductance is in series with the paralleled L-C branches, the resonant frequency depends on L_{r1}+L_{lk} resonates with C_{r1}, and the zero-gain frequency remains. Thus, the relation between two resonant inductors could be re-written. Equations (2-1) (2-2) (2-3) (3-8) are updated. Also, Figure 2.2 can be updated to Figure 3.6.

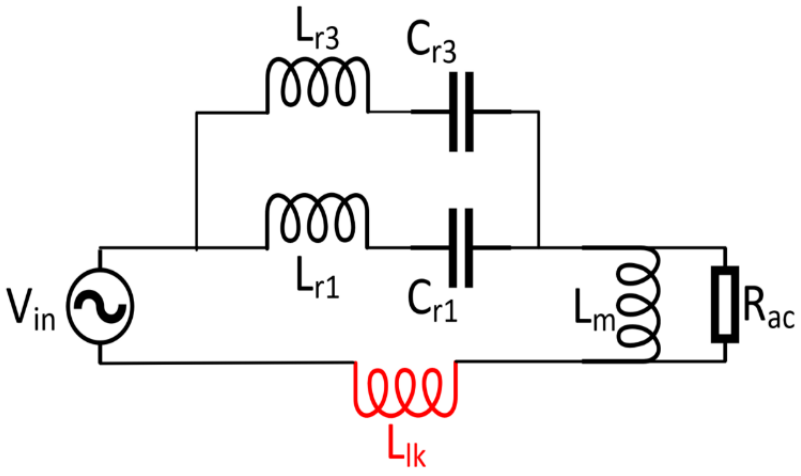

Figure 3.6 New FHA model of proposed topology

$$f_1 = \frac{1}{2\pi\sqrt{(L_{r1} + L_{lk})C_{r1}}} \quad (3-9)$$

$$f_2 = \frac{1}{2\pi\sqrt{(L_{r1} + L_{r3})\left(\frac{C_{r1}C_{r3}}{C_{r1} + C_{r3}}\right)}} \quad (3-10)$$

$$f_3 = \frac{1}{2\pi\sqrt{(L_{r3} + L_{lk})C_{r3}}} \quad (3-11)$$

$$L_{r3} = \frac{x^2 - 1}{9 - x} L_{r1} - \frac{2x^2}{9 - x^2} L_{lk} \quad (3-12)$$

If the relation between resonant frequency and zero-gain frequency is determined, then there will be only one variable to design, which is L_{r1}. Figure 2.5 shows the voltage gain curves based on different resonant inductors. With small resonant inductors, which is the blue curve in Figure 2.5, the gain curve has a very sharp notch at zero-gain frequency point, which is not friendly to the control at the low line region, and the voltage gain at high frequency is not preferred. While with large resonant inductors, which is like the green curve in Figure 2.5, the slope of the gain curve around resonant frequency is also large, which is also not good for the control. And the third harmonic current and fundamental frequency current are likely in-phase only at the unity gain point, the phase shift between two current waveforms is small. With the gain decreasing, the phase shift will be larger.

3.2 ZVS Performance

At low frequency that is close to the resonant frequency, the third harmonic current and fundamental frequency current are likely in-phase, the total resonant current is close to a semi-square wave. At high frequency, the phase shift between two harmonic currents components is significant, the total resonant current may change the direction in

one switching cycle, it will lose ZVS if the C_{oss} of the primary device does not discharge completely. Figure 3.7 shows the circuit loses ZVS at a low output voltage. From figure, the resonant current has several zero-crossing points in one switching cycle.

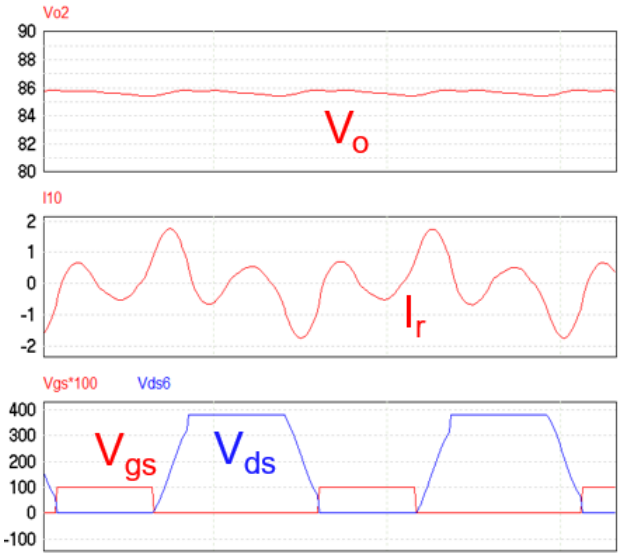

Figure 3.7 ZVS issue at low output voltage

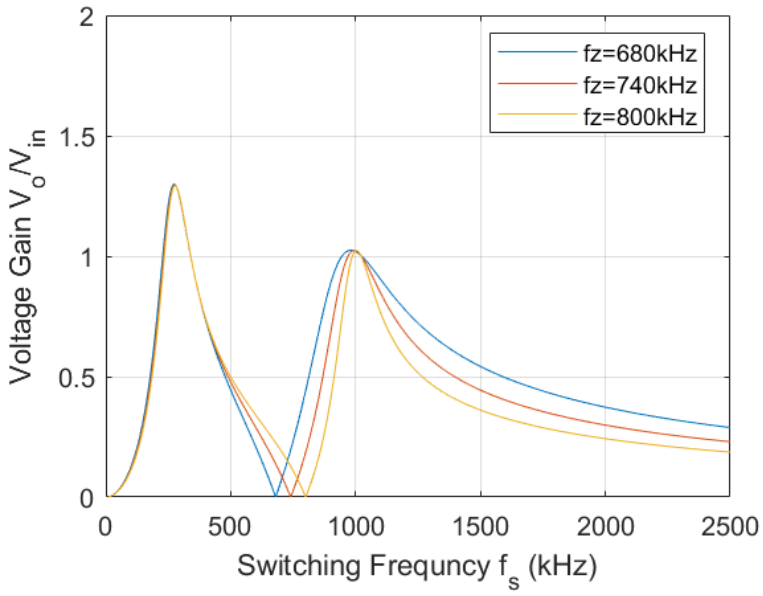

Figure 3.8 Voltage gain curves with different zero-point frequency

To solve this issue, the voltage gain of 3rd harmonics at the high frequency should be reduced. Keep the resonant frequency unchanged, push the zero-gain frequency higher. Figure 3.8 shows voltage gain curves with different zero-gain frequencies, and with a higher zero-gain frequency, the gain at high frequency is lower. Then, the circuit performance around resonant frequency does not change while the current performance at high frequency is better.

From Figure 3.9(a), the zero-gain frequency is 680 kHz, and output is 86 V, but the resonant current changes direction in a single switching cycle and it loses ZVS on the primary side. While from Figure 3.9(b), the zero-gain frequency is pushed to 740 kHz, the output is also 86 V, the circuit can achieve ZVS on the primary side. Thus, increasing the zero-gain frequency can increase the ZVS frequency range.

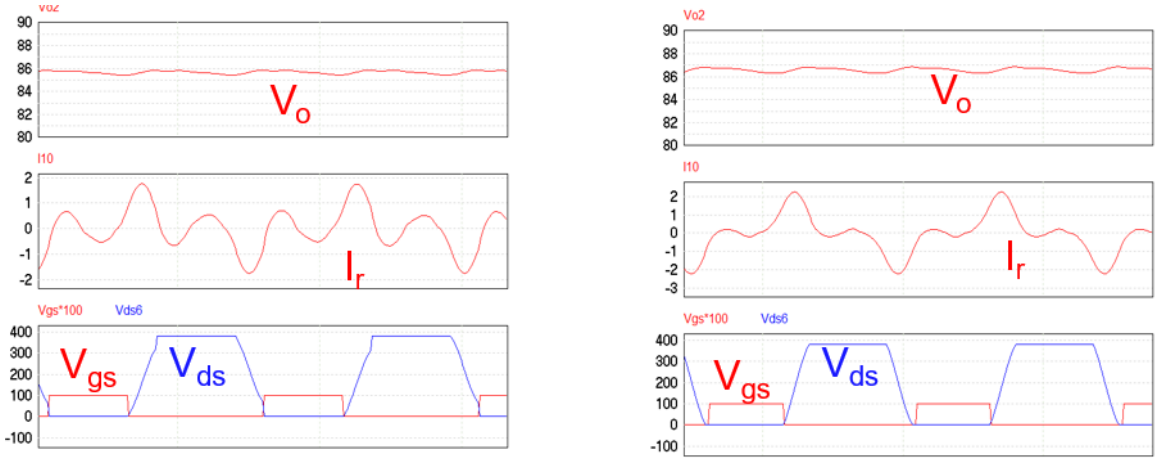

(a) (b)

Figure 3.9 ZVS conditions at same output voltage with different zero-gain frequency

Thus, the main tradeoff during the design is as followed:

(1) Push the zero-gain frequency point to be close to the second unity gain point f_3, the switching frequency range is wider while the effect of the 3rd harmonics at high switching frequency is smaller.

(2) With a smaller resonant inductor, the size of the passive components can be saved, but the effect of the 3rd harmonics at high switching frequency is larger.

3.3 Design methodology

As a summary, a flow chart of design methodology is presented below.

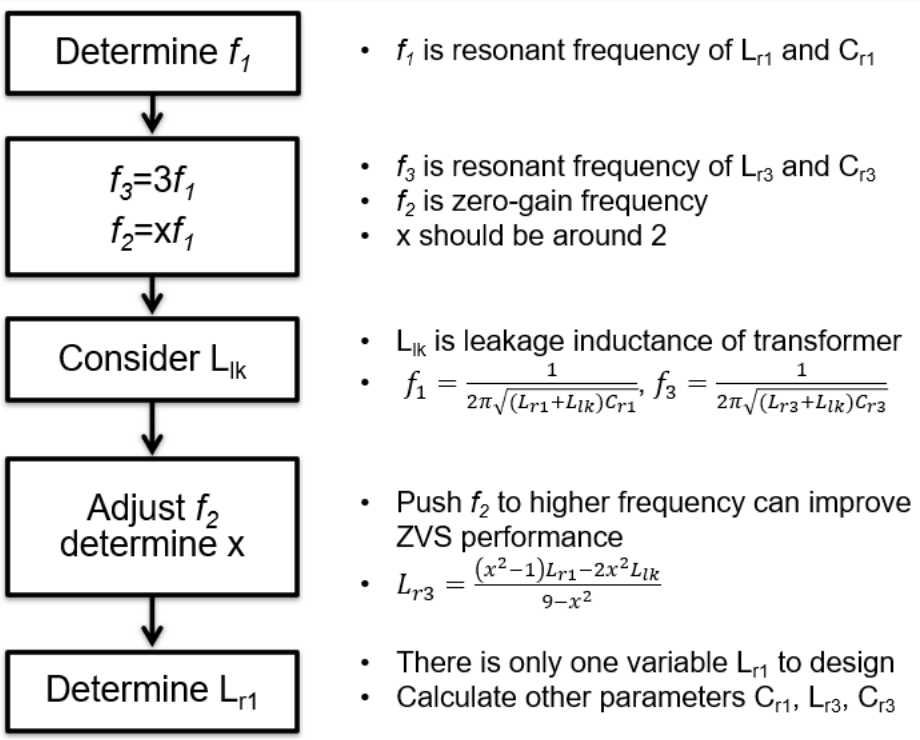

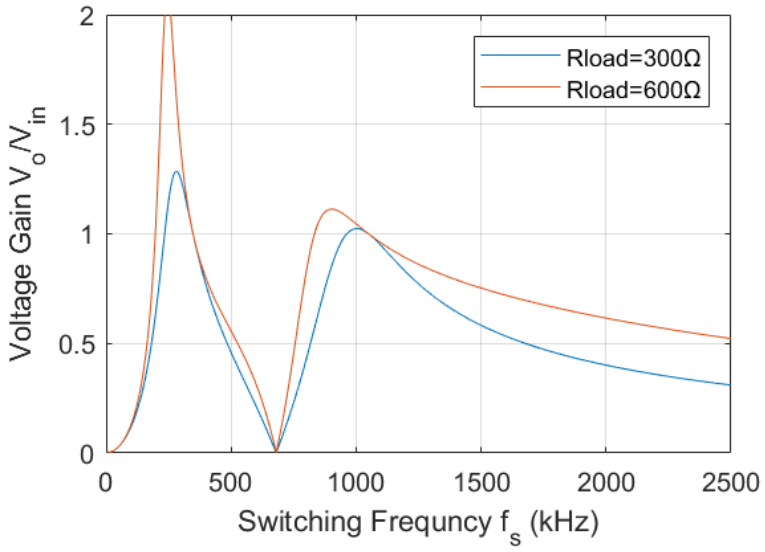

Figure 3.10 Voltage gain curves with different load condition

Besides, the different load conditions are presented in Figure 3.10. The blue curve is from full load condition that the load resistance is 300 Ω, and the orange curve is from the half load condition that the load resistance is 600 Ω. From the gain curves, the half load case has high voltage gain at high frequency which makes it harder to achieve ZVS. And the half load condition has higher 3rd harmonics gain which will affect the lowest voltage gain when the switching frequency is close to the zero-gain frequency point.

3.4 Simulation Verification

Since the zero-gain frequency is picked as 740 kHz, $f_2 = 2.17f_1$, $L_{r3} = 0.87L_{r1} - 2.22L_{lk}$ based on equation (3-12). Figure 3.11 is the updated multi-resonant LLC by adding the leakage inductor L_{lk} to Figure 2.1. The resonant elements are designed in Table 3.1. Based on equation (3-6) and parameters from Table 3.1, the weight ratio of the two current components is $\frac{I_{r3,peak}}{I_{r1,peak}} = \frac{1}{2}$.

And dc/dc simulation results are shown in Figure 3.12. The blue curves are from the single-resonant LLC while the red curves are from the proposed multi-resonant LLC. The top image shows the voltage gain of the two topologies is almost the same and the bottom image presents the resonant current performance. The shape of the resonant current of the single-resonant LLC converter is sinusoidal, while the shape of the resonant current of the multi-resonant LLC converter is a combination of two sinusoidal waveforms which are fundamental and third harmonic frequency. The rms values of resonant current of single-resonant LLC and multi-resonant LLC are 10.7 A and 8.9 A at full load, which is shown in Table 3.2. At half load, multi-resonant LLC can also save rms value of resonant current. With the same output power, multi-resonant LLC has a lower resonant current rms value so that the conduction loss of the primary side devices can be saved. Since the gain curves of single-resonant LLC and multi-resonant LLC are different except the resonant frequency point, so the comparison between the single-resonant LLC and the multi-resonant LLC is only at the resonant frequency. Then the two current components from two branches are shown in Figure 3.13. The red curve is the fundamental component that works at the resonant frequency and the blue curve is the third harmonic component. The weight ratio of the two current components is $\frac{I_{r3,peak}}{I_{r1,peak}} = \frac{7.28}{11.04} \approx \frac{2}{3}$. Figure 3.12(a) shows the full load condition, and the resonant current of multi-resonant LLC has a lower peak and lower rms value. Figure 3.12(b) represents the half load condition.

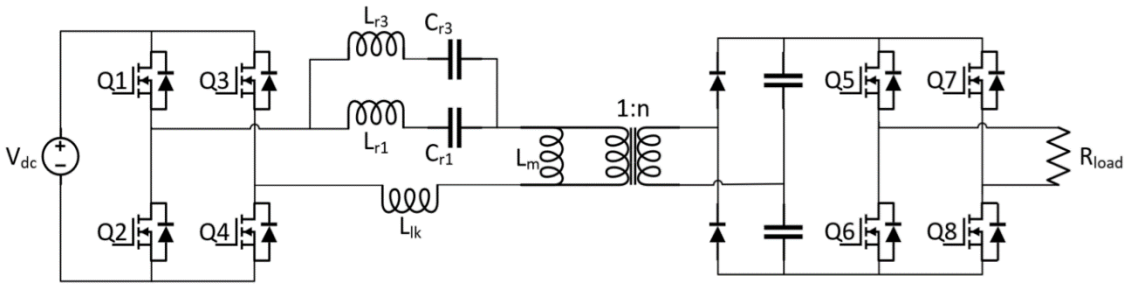

Figure 3.11 Updated multi-resonant LLC

Table 3.1 Resonant elements parameters

Parameters	**Value**
L_{r1}	30 uH
C_{r1}	6.5 nF
L_{r3}	20 uH
C_{r3}	1.06 nF
Leakage inductance L_{lk}	2.13 uH
Magnetizing inductance L_m	34 uH
Turns ratio 1: n	9:10
Resonant frequency f_r	340 kHz
Switching frequency range f_s	340 kHz – 650 kHz
V_{in}	380 V
V_o	600 V_{rms}
R_{load}	300 Ω (1.2 kW) / 600 Ω (600 W)

Table 3.2 Resonant current rms value comparison between single-resonant LLC and multi-resonant LLC at f_s=f_r

	Single-resonant LLC	**Multi-resonant LLC**
$I_{r,rms}$ @ full load condition	10.69 A	8.9 A
$I_{r,rms}$ @ half load condition	9.07 A	7.38 A

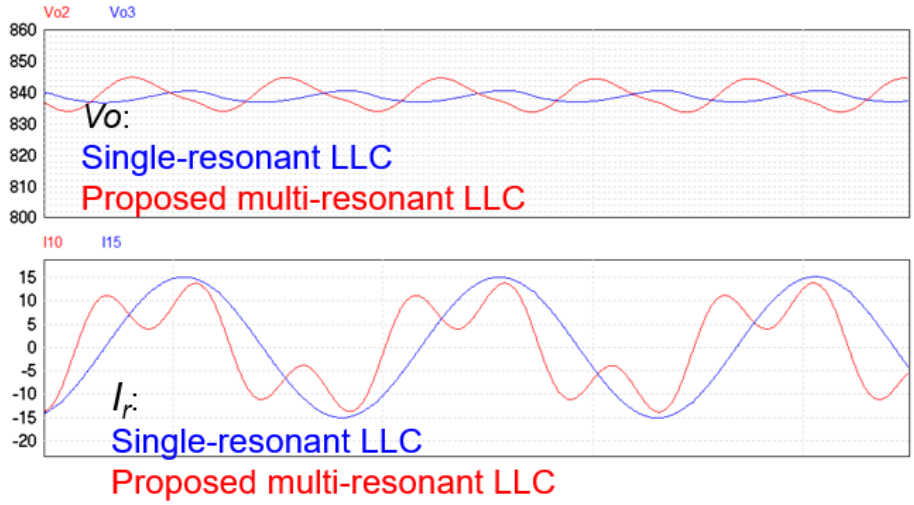

(a)

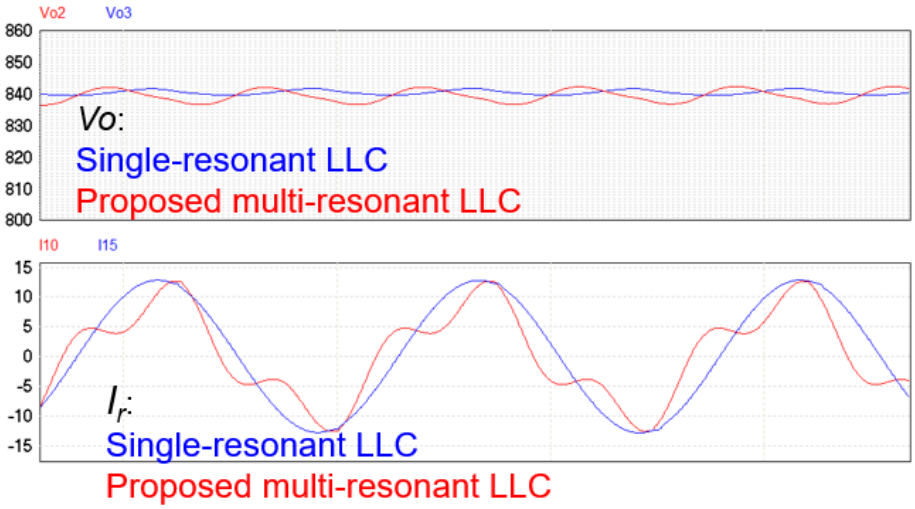

(b)

Figure 3.12 Comparison between single-resonant LLC and multi-resonant LLC with dc/dc simulation at resonant frequency (a) at full load condition; (b) at half load condition

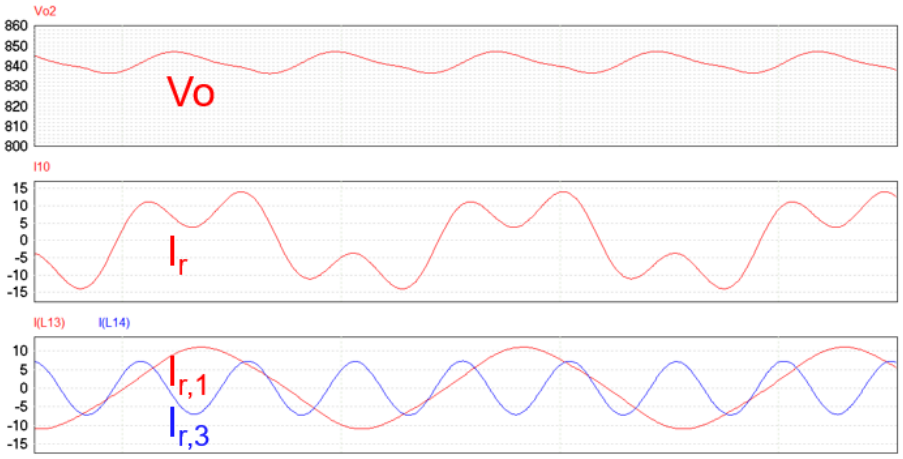

Figure 3.13 Two current components in two resonant branches from dc/dc simulation at full load condition at resonant frequency in multi-resonant LLC

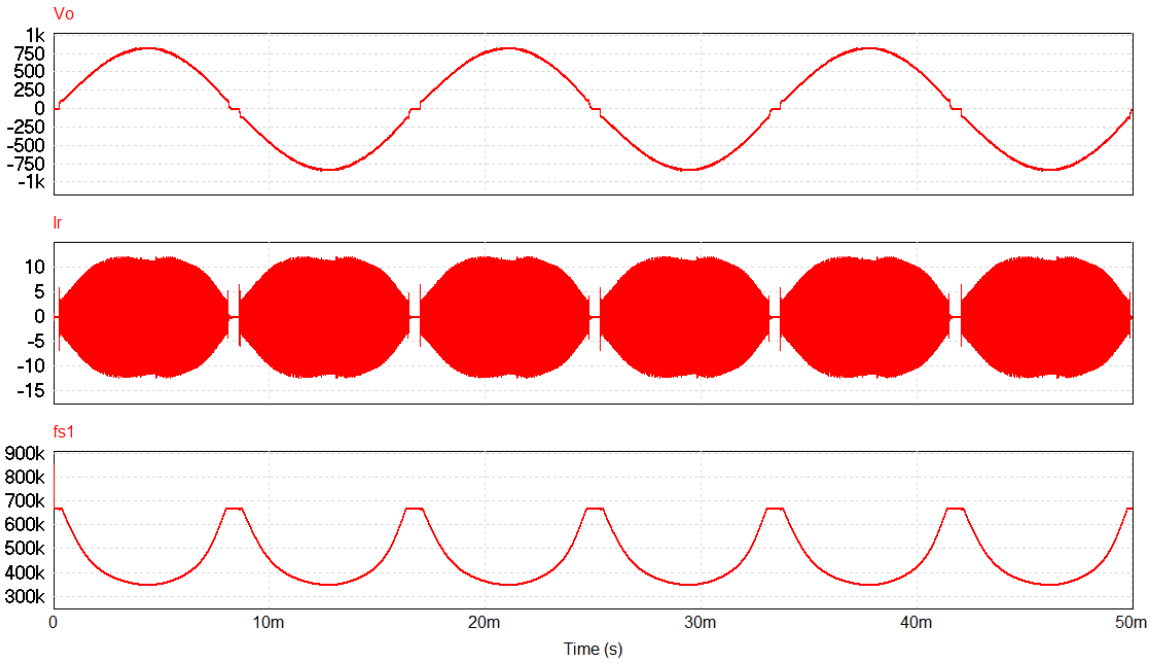

(a)

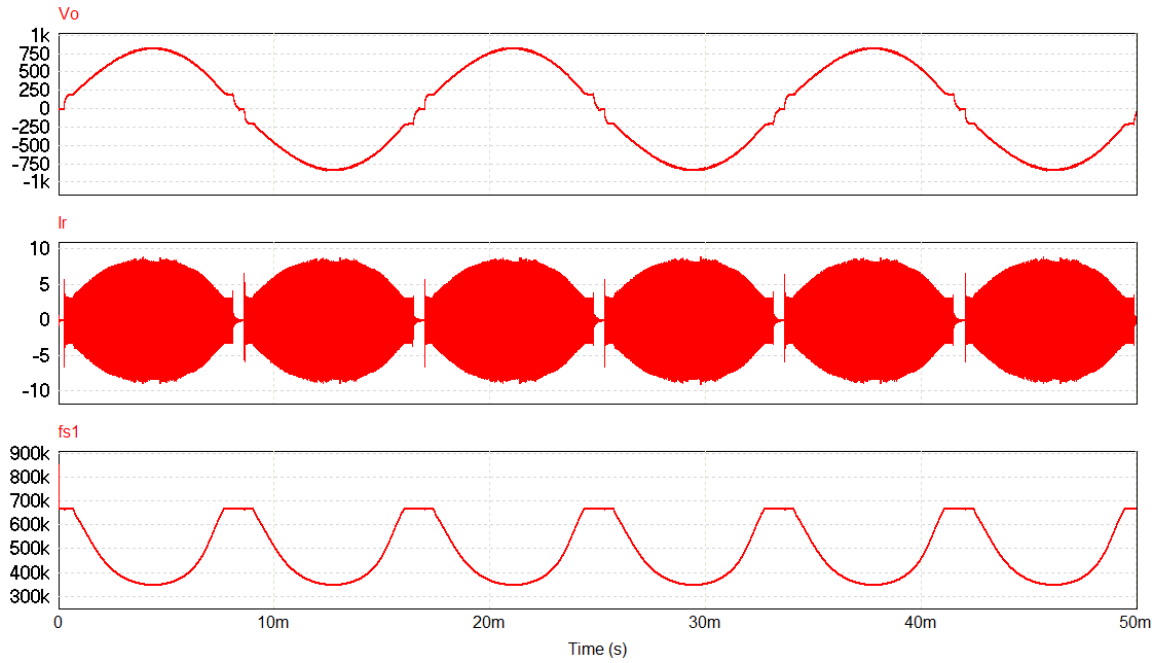

(b)

Figure 3.14 dc/ac simulation results (a) at full load condition; (b) at half load condition

Figure 3.14 presents dc/ac simulation at full load and half load. The three images are output voltage, resonant current, and switching frequency range. At full load, the output is 587.4 V_{rms} and the resonant current is 5.6 A_{rms} and THD is 2.19%, while at half load, the output voltage is 588.7 V_{rms}, the resonant current is 3.6 A_{rms} and THD is 3.81%.

Chapter 4 Experiments Results and Loss Analysis

4.1 Test Result dc/dc

A multi-resonant LLC inverter is built according to the circuit diagram in Figure 3.11. The prototype is setup for 380 V_{dc} – 600 V_{ac} at 1.2 kW output power level. The parameters are designed and adjusted following Table 3.1. And additional components information is shown in .

Table 4.1 Additional components selection

Component	**Device/Material**
Q_1-Q_4	GS66516T
Rectifying stage diode	SCS210KG
Q_5-Q_8	C3M0075120K
Core of transformer and resonant inductors	ML91S

The dc/dc conversion should be verified at first. And Figure 4.1 presents the dc/dc simulation and test result at f_s=344 kHz which is almost the resonant frequency. The test is at the full load condition, the input is 380 V_{dc} and the output is 835 V_{dc} which is the peak voltage of a sinusoidal wave with 590 V_{rms}. The light blue curve and the deep blue curve present V_{ds} and V_{gs} of one low side switch in the primary side, and the purple curve shows the resonant current in the primary side. ZVS is achieved and resonant current is a

combination of two sinusoidal waveforms. However, the two harmonics components are not completely in phase. The reason is that there is a deviation between the exact resonant frequency and the calculated resonant frequency. And the phase difference of two harmonics components grows when the switching frequency increases. The dc/dc simulation and test result at f_s=635 kHz at full load condition is shown in Figure 4.2. The input is 380 Vdc while the output is 147 Vdc which is about 17% of the peak voltage of the designed output sinusoidal wave. And ZVS is also achieved. Then the gain range is from 0.17 – 1 so the THD of output ac waveform can be expected to around 3% according to Figure 1.9.

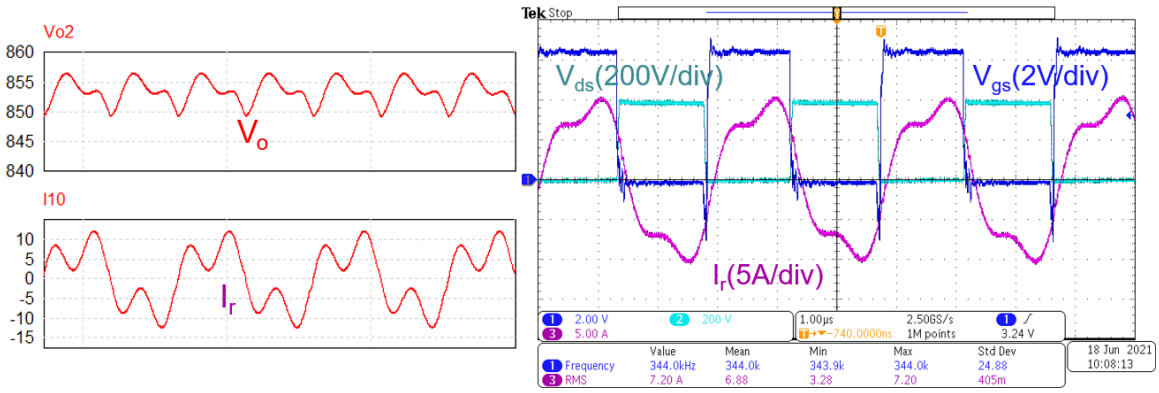

Figure 4.1 dc/dc test at f_s=344 kHz at full load condition

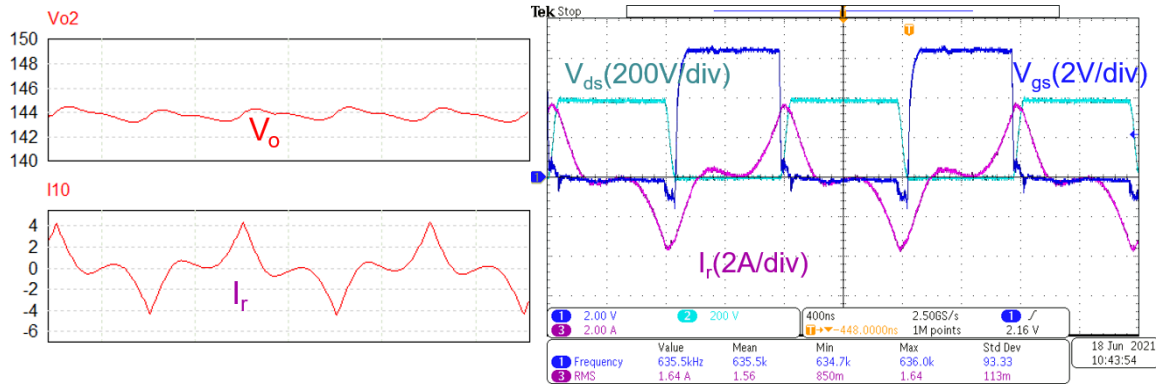

Figure 4.2 dc/dc test at f_s=635 kHz at full load condition

4.2 Test Result dc/ac

As shown in Figure 4.3 and Figure 4.4, the yellow curve is the output voltage V_o, and the red curve represents the resonant current I_r in the primary side. For the full load condition, the output is 587.4 V_{rms}, the efficiency is 97.3% and THD is 2.17%. For the half load condition, the output is 588.7 V_{rms}, the efficiency is 97.2% and THD is 3.2%. The THD at half load condition is worse because the lowest voltage gain of the half load condition is higher, so the gain range is narrower that results in a worse THD. Under different load conditions, the THD is much better than the performance of the single-resonant LLC inverter [20]. The peak of the resonant current is lower compared to the single-resonant LLC inverter.

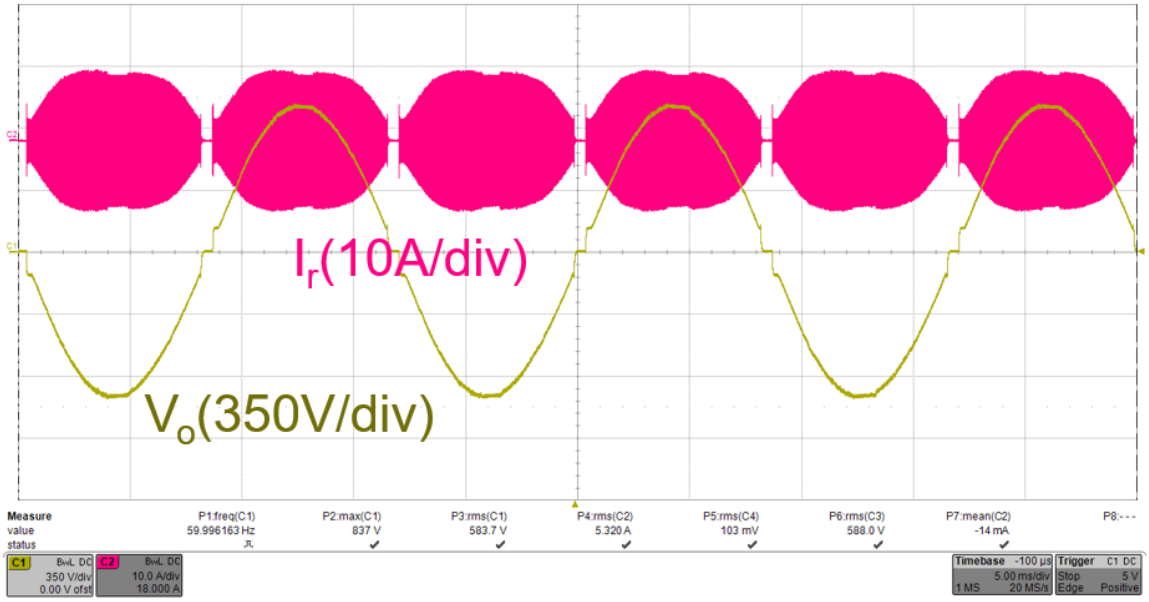

Figure 4.3 dc/ac test result at full load condition (1.2 kW)

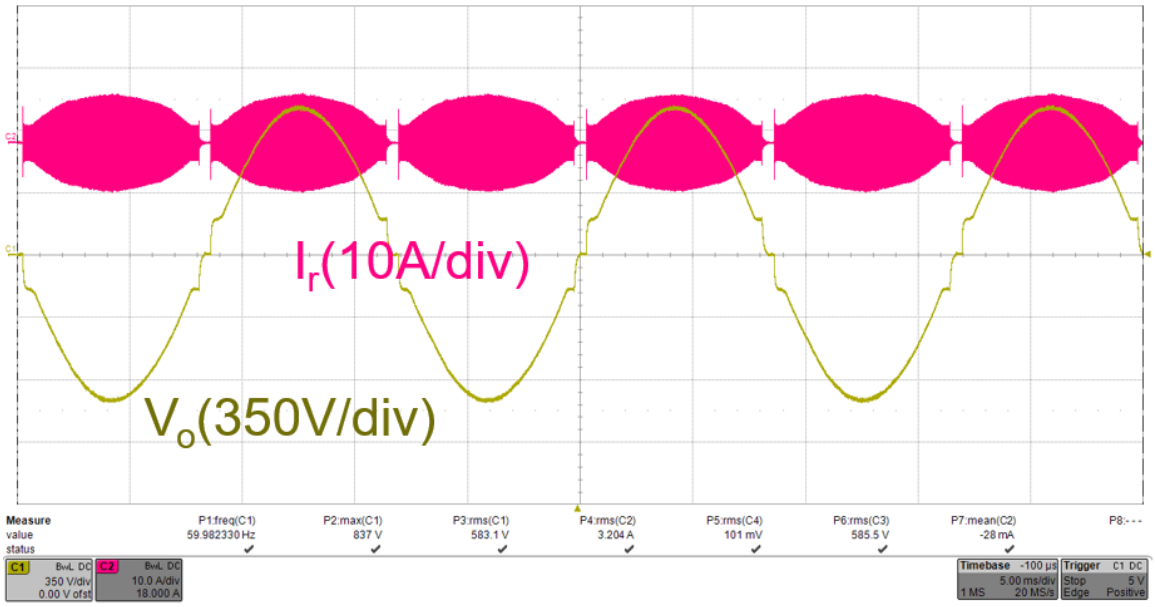

Figure 4.4 dc/ac test result at half load condition (600 W)

4.3 Loss Breakdown

The total power loss consists of conduction loss and switching loss from the primary side and secondary side, and magnetic loss from the transformer and inductors. The switching loss of the unfolding stage can be ignored since the switches of the unfolding stage works at twice line frequency which is only 120 Hz, and it is nothing comparing to the switching frequency that works at hundred-kHz level. The summary of power stage components losses is shown in Table 4.2. And the core loss of the transformer and inductors is calculated based on Figure 4.5. The core loss result is an estimation since the equation and the parameters are all based on a toroidal core. The magnetic components that used in the experiments use PQ50/50 and PQ50/35 core.

Table 4.2 Summary of power stage components losses

Primary Side Device Conduction Loss	$P_{pri,cond} = I_{pri,rms}^2 R_{ds(on)}$ $(4-1)$
Primary Side Device Switching Loss	$P_{pri,sw} = \frac{1}{2} V_{DS} I_{DS} f_s t_{sw,off}$ $(4-2)$
Rectifying Stage Diode Conduction Loss	$P_{rec,cond} = \int I_{sec} V_F$ $(4-3)$
Capacitor ESR Conduction Loss	$P_{ESR,cond} = I_{rms}^2 R_{ESR}$ $(4-4)$
Core Loss	$P_{cv} = k \cdot Bm^{\alpha} f^{\beta}$ $(4-5)$ $Bm = \frac{i_{max} L}{N A_e}$ $(4-6)$ $P_{core} = P_{cv} \times (core\ volume)$ $(4-7)$

$Pcv=k \cdot Bm^{\alpha} \cdot f^{\beta}$

Pcv : core loss (kW/m^3) k : coefficient
f : frequency (Hz) α,β : exponent
Bm : magnetic flux density (T)

	Frequency(kHz)	Temperature(℃)	k	α	β
ML95S	500-1000	23	4.098E-05	3.020	1.786
		100	8.090E-06	3.536	2.011
ML91S	500-1000	23	6.490E-06	3.335	1.938
		100	2.022E-07	3.553	2.241

・Toroidal core: OD14,ID7,TH5mm (ML95S,ML91S)
・Measurement system: SY8218 (IWATSU)
・Bm for ML91S should be less than 50 mT.

Figure 4.5 Mn-Zn ferrite core loss data from Hitachi Metals

From the experimental verifications, the measured power loss from the experiments at full load condition is 31.4 W. Based on the PSIM simulation and calculations, at full load condition that the output power is 1.2 kW, the total loss is 27.8 W, the major loss comes from secondary side conduction, transformer, and resonant inductor. Compared to the conventional single-resonant LLC converter in dc/dc conversion, the magnetic loss will be larger because of the varying switching frequency

and varying output voltage at the transformer which results in higher B_{max} and then higher core loss.

Besides, the channel turn-off loss of switches in the primary side is also larger because the turn-off current can be expected to be higher to guarantee the achievement of ZVS in the wide gain range. The difference between the loss from experiment and the loss from simulation is 3.6 W which could be from the magnetic components due to the rough core loss calculation. Loss breakdown at full load condition is presented in Table 4.3 below.

Table 4.3 Loss breakdown

	Full Load
Primary side conduction loss	1.77 W
Primary side channel turn-off loss	2.62 W
Secondary side conduction loss	7.08 W
Unfolder conduction loss	0.59 W
Transformer loss	7.27 W
External inductor L_{r1} loss	6.56 W
External inductor L_{r3} loss	0.62 W
Capacitors ESR loss (C_r, C_p & voltage doubler capacitors)	1.28 W
Total	**27.79 W**

Chapter 5 Conclusions and Future Work

5.1 Conclusions

It is proposed in this thesis that achieving a single-stage inverter based on LLC converter by using multi-resonant L-C branches. The work consists of the analysis of theoretical topology model, resonant tank design, simulation, implementation of hardware, and experimental verification. With the proposed multi-resonant LLC inverter, the switching frequency range can be narrower, the gain range of the converter can be wider and THD is better compared to the single-resonant LLC inverter. And wide-range ZVS is achieved compared to other inverters which use PDM modulation method.

There are two L-C resonant branches, the first branch resonates at the fundamental resonant frequency, and the second branch is responsible for three times of fundamental frequency. The merits of the proposed resonant tank are wide zero gain range and power delivery capability.

The voltage gain can be theoretically close to zero so that the wide voltage output range can be achieved in a limited switching frequency and good THD can be obtained at different load conditions. In the conventional single-resonant LLC converter, switching frequency would go to MHz level to get a low voltage gain even with half-bridge mode, while the multi-resonant LLC can get a quite low voltage output at around twice the resonant frequency. Also, the control method can be simpler, and a combination of different modes is not needed.

The dc/dc simulations working at resonant frequency are made to compare the conventional single-resonant LLC converter and proposed multi-resonant LLC converter.

The resonant current of the proposed multi-resonant LLC converter has a lower amplitude and a lower rms value at $f_s=f_r$, in dc/dc conversion. It can save 16.7% current rms at full load and 18.6% at half load. The dc/ac simulations are made for loss breakdown analysis. The demerit of the design is the magnetic loss of the additional L-C resonant branch.

A prototype is built to verify the design and it achieves 97.3% efficiency and 2.17% THD at full load condition, and 97.2% efficiency and 3.2% THD are achieved at half load condition.

5.2 Future Work

Most analysis in this thesis is based on fundamental harmonics approximation and the model is only accurate at the resonant frequency, and the 3rd harmonics component is only taken into consideration at $f_s=f_r$ in dc/dc conversion. The reason is that the fundamental harmonics and 3rd harmonics are in phase only at the switching frequency equal to the resonant frequency while there will be a phase difference between the fundamental component and 3rd harmonics component when $f_s>f_r$. Then the effect of 3rd harmonic is hard to estimate, and the 3rd harmonic component is usually avoided in the design. However, higher-order harmonics can help deliver power with an appropriate design. Thus, a model could be developed to show an accurate gain curve of the resonant converter that combines the effect of fundamental component and higher-order harmonics components.

In the thesis, the load is constant-resistance load, so the control strategy is easy and only a voltage control loop is needed. And this prototype can be developed to be a grid-

tied inverter. And then the control strategy should be modified, and a current control loop should be included.

Reference

[1] Zeb, Kamran, Waqar Uddin, Muhammad Adil Khan, Zunaib Ali, Muhammad Umair Ali, Nicholas Christofides, and H. J. Kim. "A comprehensive review on inverter topologies and control strategies for grid connected photovoltaic system." *Renewable and Sustainable Energy Reviews* 94 (2018): 1120-1141.

[2] Tian, Feng, Hussam Al-Atrash, Rene Kersten, Charles Scholl, Kasemsam Siri, and Issa Batarseh. "A single-staged PV array-based high-frequency link inverter design with grid connection." In *Twenty-First Annual IEEE Applied Power Electronics Conference and Exposition, 2006. APEC'06.*, pp. 4-pp. IEEE, 2006.

[3] Mao Xingkui, Huang Qisheng, Ke Qingbo, Xiao Yudi, Zhang Zhe and M. A. E. Andersen, "Grid-connected photovoltaic micro-inverter with new hybrid control LLC resonant converter," in *Proc. Annu. Conf. IEEE Ind. Electron. Soc.*, Oct. 2016, pp. 2319-2324.

[4] H. Hu, S. Harb, N. Kutkut, I. Batarseh and Z. J. Shen, "A Review of Power Decoupling Techniques for Microinverters With Three Different Decoupling Capacitor Locations in PV Systems," *IEEE Trans. Power Electron.*, vol. 28, no. 6, pp. 2711-2726, June 2013.

[5] X. Zhao, L. Zhang, R. Born and J. Lai, "Solution of input double-line frequency ripple rejection for high-efficiency high-power density string inverter in photovoltaic application," in *Proc. IEEE Appl. Power Electron. Conf. Expo.*, Mar. 2016, pp. 1148-1154.

[6] M. A. Rezaei, K. Lee and A. Q. Huang, "A High-Efficiency Flyback Micro-inverter With a New Adaptive Snubber for Photovoltaic Applications," in IEEE Transactions on Power Electronics, vol. 31, no. 1, pp. 318-327, Jan. 2016.

[7] B. Han, J. S. Lee and M. Kim, "Repetitive Controller With Phase-Lead Compensation for Cuk CCM Inverter," in IEEE Transactions on Industrial Electronics, vol. 65, no. 3, pp. 2356-2367, March 2018.

[8] Caceres, Ramon O., and Ivo Barbi. "A boost DC-AC converter: analysis, design, and experimentation." *IEEE transactions on power electronics* 14, no. 1 (1999): 134-141.

[9] Kusakawa, Masato, Hiroshi Nagayoshi, Koichi Kamisako, and Kosuke Kurokawa. "Further improvement of a transformerless, voltage-boosting inverter

for ac modules." *Solar Energy Materials and Solar Cells* 67, no. 1-4 (2001): 379-387.

[10] Ahmed, Nabil A., Hyun Woo Lee, and Mutsuo Nakaoka. "Dual-mode time-sharing sinewave-modulation soft switching boost full-bridge one-stage power conditioner without electrolytic capacitor DC link." *IEEE Transactions on Industry Applications* 43, no. 3 (2007): 805-813.

[11] Madouh, Jamal, Nabil A. Ahmed, and Ahmad M. Al-Kandari. "Advanced power conditioner using sinewave modulated buck–boost converter cascaded polarity changing inverter." *International Journal of Electrical Power & Energy Systems* 43, no. 1 (2012): 280-289.

[12] Jain, Sachin, and Vivek Agarwal. "A single-stage grid connected inverter topology for solar PV systems with maximum power point tracking." *IEEE transactions on power electronics* 22, no. 5 (2007): 1928-1940.

[13] Panguloori, RakeshBabu, Debaprasad Kastha, Amit Patra, and Giovanni Capodivacca. "High performance voltage regulator for high step-down DC-DC conversion." In *2008 34th Annual Conference of IEEE Industrial Electronics*, pp. 761-765. IEEE, 2008.

[14] J.-S. Lai, M. Lee, C.-S. Yeh, B. Gutierrez, Z. Hou, H. Wen, D. Jiao and H. Hsieh, "A Hybrid Binary Multilevel Cascaded Inverter for Medium-Voltage Applications," Proc. IEEE ECCE, Vancouver, Canada, Oct. 2021.

[15] Yeh, Chih-Shen, Oscar Yu, and Jih-Sheng Lai. "Sequential Waveform Synthesis for Multi-Modular SRC-Unfolding Inverter." *IEEE Journal of Emerging and Selected Topics in Power Electronics* (2020).

[16] Yang, Bo, Fred C. Lee, A. J. Zhang, and Guisong Huang. "LLC resonant converter for front end DC/DC conversion." In *APEC. Seventeenth Annual IEEE Applied Power Electronics Conference and Exposition (Cat. No. 02CH37335)*, vol. 2, pp. 1108-1112. IEEE, 2002.

[17] Lu, Bing, Wenduo Liu, Yan Liang, Fred C. Lee, and Jacobus D. Van Wyk. "Optimal design methodology for LLC resonant converter." In *Twenty-First Annual IEEE Applied Power Electronics Conference and Exposition, 2006. APEC'06.*, pp. 6-pp. IEEE, 2006.

[18] Fu, Dianbo, Bing Lu, and Fred C. Lee. "1MHz high efficiency LLC resonant converters with synchronous rectifier." In *2007 IEEE Power Electronics Specialists Conference*, pp. 2404-2410. IEEE, 2007.

[19] B. Yang, F. C. Lee, A. J. Zhang, G. Huang, “LCL resonant converter for front end DC/DC conversion,” Proc. IEEE APEC, vol. 2, pp. 1108–1112, 2002.

[20] Wen, Hao. *High-Efficiency and High-Frequency Resonant Converter Based Single-Stage Soft-Switching Isolated Inverter Design and Optimization with Gallium-Nitride (GaN)*. Diss. Virginia Tech, 2021.

[21] R. Chaffai, K. Al-Haddad and V. Rajagopalan, "A 5 kW utility-interactive inverter operating at high frequency and using zero current turn off COMFET switches," *Conference Record of the 1990 IEEE Industry Applications Society Annual Meeting*, Seattle, WA, USA, 1990, pp. 1081-1085 vol.2.

[22] Fu, Dianbo, Fred C. Lee, Ya Liu, and Ming Xu. "Novel multi-element resonant converters for front-end dc/dc converters." In *2008 IEEE Power Electronics Specialists Conference*, pp. 250-256. IEEE, 2008.

[23] Shepherd, William, and P. Zand. *Energy flow and power factor in nonsinusoidal circuits*. Cambridge University Press, 1979.

[24] Elrayyah, Ali. "LLC Converters Power Density Enhancement through Optimized Current Shaping Using Multi-Resonant Branches." In *2020 IEEE Energy Conversion Congress and Exposition (ECCE)*, pp. 370-376. IEEE, 2020.

[25] D. Huang, F. C. Lee and D. Fu “Classification and selection methodology for multi-element resonant converters,” Proc. IEEE APEC, pp. 558–565, 2011.

[26] J. Koscelnik, M. Frivaldsky, M. Prazenica and R. Mazgut, “A review of multi-elements resonant converters topologies,” Proc. ELEKTRO Conf., pp. 312–317, 2014.

[27] Y. Wang, F. Han, L. Yang, R. Xu and R. Liu, “A three-port bidirectional multi-element resonant converter with decoupled power flow management for hybrid energy storage,” IEEE Access, vol. 6 pp. 61331–61341, 2018.

[28] J. Y. Lin, Y. F. Lin, and S. Y. Lee, “A Novel Multi-Element Resonant Converter with Self-Driven Synchronous Rectification,” Energies, vol. 12, no. 4, 715, 2019.

[29] R. W. Erickson and D. Maksimovic, Fundamentals of Power Electronics, 2nd ed. New York: Springer, 2001.

[30] N. Shafiei, M. A. Saket, and M. Ordonez, “Time domain analysis of LLC resonant converters in the boost mode for battery charger applications,” in Proc. IEEE Energy Convers. Congr. Expo., Oct. 2017, pp. 4157–4162.

[31] E. S. Glitz, M. Amyotte, M. C. G. Perez, and M. Ordonez, “LLCconverters: Beyond datasheets for MOSFET power loss estimation,” in Proc. IEEE Appl. Power Electron. Conf. Expo., Mar. 2018, pp. 464–468.

[32] Glitz, Ettore Scabeni, and Martin Ordonez. "MOSFET power loss estimation in LLC resonant converters: Time interval analysis." *IEEE Transactions on Power Electronics* 34, no. 12 (2019): 11964-11980.

[33] Wen, Hao, Dong Jiao, Jih-Sheng Lai, Johan Strydom, and Lanhua Zhang. "An Accurate Voltage Gain Model Considering Diode Effect for LLC Resonant Converter in Wide Gain Range Applications." In *2020 IEEE Energy Conversion Congress and Exposition (ECCE)*, pp. 5436-5441. IEEE, 2020.

[34] Yan, Chao, Fan Li, Jianhong Zeng, Teng Liu, and Jianping Ying. "A novel transformer structure for high power, high frequency converter." In *2007 IEEE Power Electronics Specialists Conference*, pp. 214-218. IEEE, 2007.